

Министерство науки и высшего образования Российской Федерации
ФЕДЕРАЛЬНОЕ ГОСУДАРСТВЕННОЕ АВТОНОМНОЕ ОБРАЗОВАТЕЛЬНОЕ
УЧРЕЖДЕНИЕ ВЫСШЕГО ОБРАЗОВАНИЯ
НАЦИОНАЛЬНЫЙ ИССЛЕДОВАТЕЛЬСКИЙ УНИВЕРСИТЕТ ИТМО
ITMO University

ВЫПУСКНАЯ КВАЛИФИКАЦИОННАЯ РАБОТА
GRADUATION THESIS

Термооптическая бистабильность в метаповерхностях, поддерживающих связанные состояния в континууме / Thermooptical Bistability in Metasurfaces Supporting Bound States in the Continuum

Обучающийся / Student Пашина Олеся Игоревна
Факультет/институт/кластер/ Faculty/Institute/Cluster физический факультет
Группа/Group Z42761
Направление подготовки/ Subject area 16.04.01 Техническая физика
Образовательная программа / Educational program Техническая физика / Physics and engineering 2021
Язык реализации ОП / Language of the educational program Русский, Английский
Статус ОП / Status of educational program МОП
Квалификация/ Degree level Магистр
Руководитель ВКР/ Thesis supervisor Петров Михаил Игоревич, PhD, физико-математические науки, Университет ИТМО, физический факультет, старший научный сотрудник

Обучающийся/Student

Документ подписан	
Пашина Олеся Игоревна	
22.05.2023	

(эл. подпись/ signature)

Пашина Олеся
Игоревна

(Фамилия И.О./ name
and surname)

Руководитель ВКР/
Thesis supervisor

Документ подписан	
Петров Михаил Игоревич	
22.05.2023	

(эл. подпись/ signature)

Петров Михаил
Игоревич

(Фамилия И.О./ name
and surname)

**Министерство науки и высшего образования Российской Федерации
ФЕДЕРАЛЬНОЕ ГОСУДАРСТВЕННОЕ АВТОНОМНОЕ ОБРАЗОВАТЕЛЬНОЕ
УЧРЕЖДЕНИЕ ВЫСШЕГО ОБРАЗОВАНИЯ
НАЦИОНАЛЬНЫЙ ИССЛЕДОВАТЕЛЬСКИЙ УНИВЕРСИТЕТ ИТМО
ITMO University**

**АННОТАЦИЯ
ВЫПУСКНОЙ КВАЛИФИКАЦИОННОЙ РАБОТЫ
SUMMARY OF A GRADUATION THESIS**

Обучающийся / Student Пашина Олеся Игоревна

Факультет/институт/кластер/ Faculty/Institute/Cluster физический факультет

Группа/Group Z42761

Направление подготовки/ Subject area 16.04.01 Техническая физика

Образовательная программа / Educational program Техническая физика / Physics and engineering 2021

Язык реализации ОП / Language of the educational program Русский, Английский

Статус ОП / Status of educational program МОП

Квалификация/ Degree level Магистр

Тема ВКР/ Thesis topic Термооптическая бистабильность в метаповерхностях, поддерживающих связанные состояния в континууме / Thermo-optical Bistability in Metasurfaces Supporting Bound States in the Continuum

Руководитель ВКР/ Thesis supervisor Петров Михаил Игоревич, PhD, физико-математические науки, Университет ИТМО, физический факультет, старший научный сотрудник

**ХАРАКТЕРИСТИКА ВЫПУСКНОЙ КВАЛИФИКАЦИОННОЙ РАБОТЫ
DESCRIPTION OF THE GRADUATION THESIS**

Цель исследования / Research goal

Исследование термооптической бистабильности в мембранах, поддерживающих связанные состояния в континууме/Investigation of thermo-optical bistability in membranes supporting bound states in the continuum

Задачи, решаемые в ВКР / Research tasks

Investigate the optical heating of the nanostructure taking into account the temperature dependence of the complex refractive index of the material; explain the thermo-optical nonlinearity and bistability based on a simple analytical model; derive various parameters of the above-mentioned nonlinearity and bistability; apply the developed model to describe the temperature evolution of the experimental periodic structure with high-Q resonance; compare the experimental and theoretically predicted results.

Краткая характеристика полученных результатов / Short summary of results/findings

In this work, thermo-optical nonlinearity and bistability were explained in terms of the model of a nonlinear single-mode resonator. We also demonstrated the bistability appearance condition and expressed such experimentally important parameters as the width and height of the hysteresis. Moreover, we provided the critical coupling condition for radiative and nonradiative losses, which maximizes the hysteresis width and underlies the effective achievement of the bistability regime in the case of an experimental implementation limited by a fixed maximum laser

pumping. Finally, we apply the developed model of a nonlinear resonator to describe the temperature evolution inside the dielectric metasurface with bound states in the continuum and obtain good agreement between the experimentally measured and analytically obtained results. In addition, we also predict the optimal excitation conditions to achieve the maximum possible hysteresis width that can be obtained in such membrane system.

Наличие публикаций по теме выпускной работы / Publications on the topic of the thesis

1. Ryabov D., Pashina O., Zograf G., Makarov S., Petrov M. Nonlinear optical heating of all-dielectric super-cavity: efficient light-to-heat conversion through giant thermorefractive bistability//Nanophotonics, 2022, Vol. 11, No. 17, pp. 3981-3991 (Статья; Scopus, Web of Science)
2. Рябов Д.Р., Pashina O. Thermo-optical bistability in single semiconductor super-cavity//Book of abstracts for "The third edition of the School of Plasmonics and Nano-Optics", 2022 (Тезисы)

Наличие выступлений на конференциях по теме выпускной работы / Conference reports on the topic of the thesis

1. The third edition of the School of Plasmonics and Nano-Optics, 04.07.2022 - 07.07.2022 (Конференция, статус - международный)

Обучающийся/Student

Документ подписан	
Пашина Олеся Игоревна	
22.05.2023	

(эл. подпись/ signature)

Пашина Олеся
Игоревна

(Фамилия И.О./ name
and surname)

Руководитель ВКР/
Thesis supervisor

Документ подписан	
Петров Михаил Игоревич	
22.05.2023	

(эл. подпись/ signature)

Петров Михаил
Игоревич

(Фамилия И.О./ name
and surname)

**Министерство науки и высшего образования Российской Федерации
ФЕДЕРАЛЬНОЕ ГОСУДАРСТВЕННОЕ АВТОНОМНОЕ ОБРАЗОВАТЕЛЬНОЕ
УЧРЕЖДЕНИЕ ВЫСШЕГО ОБРАЗОВАНИЯ
НАЦИОНАЛЬНЫЙ ИССЛЕДОВАТЕЛЬСКИЙ УНИВЕРСИТЕТ ИТМО
ITMO University**

**ЗАДАНИЕ НА ВЫПУСКНУЮ КВАЛИФИКАЦИОННУЮ РАБОТУ /
OBJECTIVES FOR A GRADUATION THESIS**

Обучающийся / Student Пашина Олеся Игоревна

Факультет/институт/кластер/ Faculty/Institute/Cluster физический факультет

Группа/Group Z42761

Направление подготовки/ Subject area 16.04.01 Техническая физика

Образовательная программа / Educational program Техническая физика / Physics and engineering 2021

Язык реализации ОП / Language of the educational program Русский, Английский

Статус ОП / Status of educational program МОП

Квалификация/ Degree level Магистр

Тема ВКР/ Thesis topic Термооптическая бистабильность в метаповерхностях, поддерживающих связанные состояния в континууме / Thermo-optical bistability in metasurfaces supporting bound states in the continuum

Руководитель ВКР/ Thesis supervisor Петров Михаил Игоревич, PhD, физико-математические науки, Университет ИТМО, физический факультет, старший научный сотрудник

Основные вопросы, подлежащие разработке / Key issues to be analyzed

Research aim:

Theoretical investigation of nonlinear optical heating and thermo-optical bistability in membranes supporting bound states in the continuum.

Work content:

- Development of an analytical model for optical heating of nanostructured systems based on the coupled-mode model of a single-mode resonator [1,2] in steady regime and taking into account the change in the complex refractive index.

- Generalization of the critical coupling condition [3], which provides the maximum heating of the system, for the non-linear case.

- Study of thermo-optical bistability resulting from the introduction of nonlinearity into the system, as well as its parameters and conditions of occurrence.

- Identification of critical conditions for the effective achievement of system bistability.

- Application of the resulting analytical model to metasurfaces supporting a high-quality quasi-BIC mode.

- Comparison of theoretical (from the developed analytical model) and experimental data of bistability in silicon metasurfaces obtained earlier by colleagues.

Recommended materials:

- [1] Hermann Haus. Waves and fields in optoelectronics.
- [2] Wonjoo Suh, Zheng Wang, and Shanhui Fan. Temporal coupled-mode theory and the presence of non-orthogonal modes in lossless multimode cavities. IEEE Journal of Quantum Electronics
- [3] Zograf et al. (2017) Resonant Nonplasmonic Nanoparticles for Efficient Temperature-Feedback Optical Heating Nano Letters

Дата выдачи задания / Assignment issued on: 15.01.2023

Срок представления готовой ВКР / Deadline for final edition of the thesis 20.03.2023

Характеристика темы ВКР / Description of thesis subject (topic)

Тема в области фундаментальных исследований / Subject of fundamental research: да / yes

СОГЛАСОВАНО / AGREED:

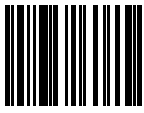
Руководитель ВКР/
Thesis supervisor

Документ подписан	
Петров Михаил Игоревич	
09.03.2023	

(эл. подпись)

Петров Михаил
Игоревич

Задание принял к
исполнению/ Objectives
assumed BY

Документ подписан	
Пашина Олеся Игоревна	
17.03.2023	

(эл. подпись)

Пашина Олеся
Игоревна

Руководитель ОП/ Head
of educational program

Документ подписан	
Белов Павел Александрович	
18.05.2023	

(эл. подпись)

Белов Павел
Александрович

CONTENTS

INTRODUCTION	7
Optical bistability	7
Hystorical background	8
Overview of bistable platforms	11
Thermo-optical effects	14
The aim of work	15
1 MODEL OF OPTICAL HEATING	19
1.1 Single mode resonator model	19
1.1.1 Linear resonator model	19
1.1.2 Nonlinear resonator model	20
1.1.3 Introduction of dimensionless quantities	21
1.1.4 Nonlinear coefficients	22
1.2 Optimal heating condition	25
1.2.1 Linear critical coupling	25
1.2.2 Nonlinear critical coupling	26
2 THERMO-OPTICAL BISTABILITY	28
2.1 Bistability effect	28
2.2 Bistability condition	29
2.3 Hysteresis parameters	31
3 BISTABILITY EXISTENCE AREA AND CRITICAL COUPLING CONDITION	36
3.1 Bistability existence area	36
3.2 Efficient reaching of bistability regime	37
3.3 Maximization of hysteresis width	38
4 BISTABILITY IN METASURFACES	42
4.1 Quasi-BIC mode	42
4.2 Temperature estimation	44
4.3 Temperature evolution of metasurfaces	45
4.4 Fitting metasurface parameters	48
4.5 Critical coupling in metasurfaces	53
CONCLUSION	55
REFERENCES	57

INTRODUCTION

Nanophotonics is an actively developing field of modern optics that investigates the interaction of light with matter at the nanoscale. Studies of this field of photonics open up promising opportunities for controlling, amplifying, transforming and generating light with proper analysis of the propagation of electromagnetic waves through such structures, and also demonstrate new physical phenomena arising from the interaction of optical radiation with nano and micro-objects. The control of light by all-optical means has always been a fundamental and most studied problem in nanophotonics, since this process can become a key effect in optical switching and logic.

So, in this work, we investigate the effect of thermo-optical bistability from the theoretical point of view and apply the developed model to the experimentally observed hysteresis behavior of structure heating, which occurs in resonant all-dielectric metasurface membranes and is enhanced by bound states in the continuum (BIC) with high quality factor.

Optical bistability

Bistability is the property of a system to possess two stable states under the same conditions. In the optical case, this means that, depending on the intensity of the incident light and the initial state, the system can be in two various states of its output signal, which can be the key to the creation of logical devices such as optical adapters, switchers, and optical memory elements [1].

Optical bistability could be observed in case of light interaction with optically nonlinear systems. At the same time, optical nonlinearity manifests itself in the nonlinear dependence of the output intensity on the input parameters and arises due to the fact that some properties of the structure are influenced by the excitation intensity. For certain settings, such systems switch from the strong nonlinearity state to the bistability mode. In this case, an optically bistable structure is called absorptive or dispersive [2], depending on whether the feedback in the system causing the bistability is associated with an intensity-dependent absorption $\alpha(I)$ (or simply $k(I)$) (for example, saturable absorption) or with an intensity-dependent refractive

index $n(I)$ (nonlinear dispersion). In the early works, which will be discussed below, these types of the effect were mainly investigated separately from each other. However, in general, these mechanisms should be taken into account simultaneously, since in many structures both dispersive and absorptive changes make a crucial contribution to bistability.

Hystorical background

Here we would like to mention some historical information about the study of optical bistability in early works. The first proposal to observe this effect in an interferometer containing a saturable absorbing medium was made by Szöke et al. in 1969 [3]. Moreover, in this paper, the authors also derived the bistability condition necessary for its observation. This article has been followed by a series of theoretical papers analyzing optical bistability with an absorptive mechanism [4], as well as the application of this approach to various saturating absorbers, such as organic dyes [5]. For some time, the experimental demonstration of the theoretically described effect was not successful, until in 1976 McCall and Gibbs observed the optical bistability in sodium vapor [6]. However, the main bistability mechanism in this work was dispersive rather than absorptive. A little later, the dispersive mechanism of bistability was also demonstrated in a system with Kerr nonlinearity $n(I) = n_0 + n_2I$ [7]. Finally, the first observation of optical bistability in semiconductors was obtained in 1979 by Gibbs due to the dispersion mechanism [8]. In this work, the optical bistability of the GaAs structure arose from the nonlinear refractive index near the excited exciton resonance of the system.

Now, let's consider the simplest model of optical bistability caused by the passage of light through an optical cavity filled with an absorbing medium, which is well described in extensive books on optical bistability [2, 9].

In above books, the authors describe the optical bistability, which reveals as a function of the transmission signal for Fabry-Perot resonator, shown in the Figure 1 a), on the incident light intensity in the stationary regime due to the presence of mirrors and an absorbing medium in the optical cavity.

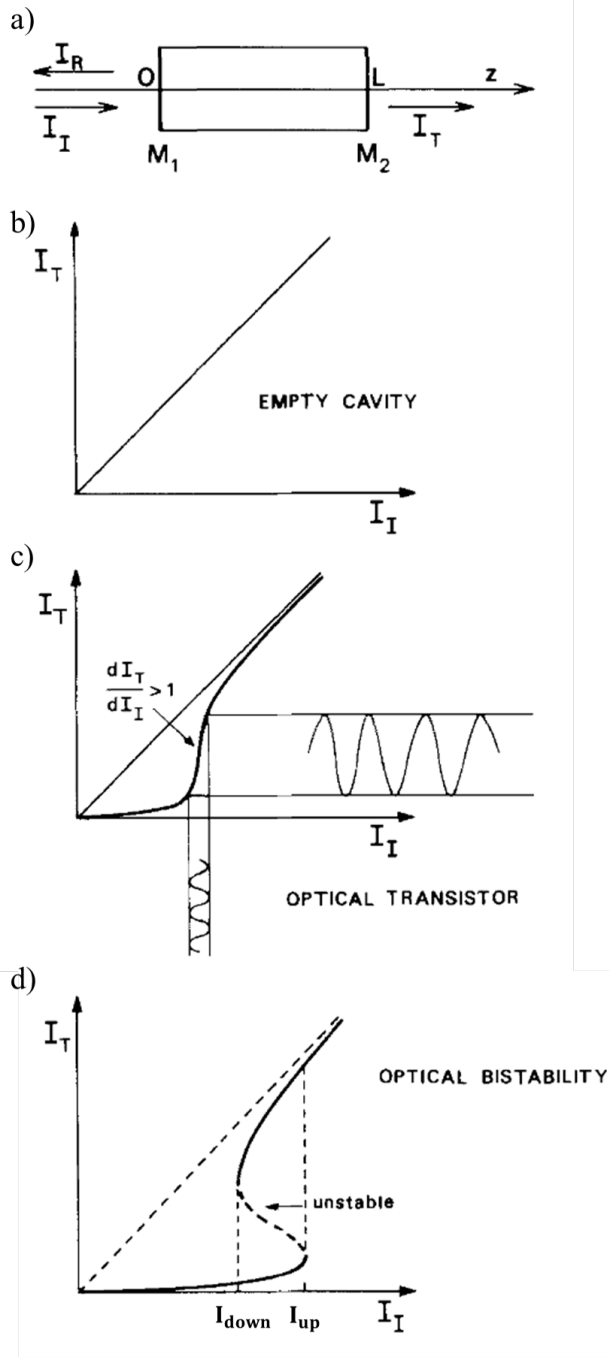


Figure 1 — a) Fabry-Perot resonator. Denoted I_I is the intensity of the incident radiation, and I_R and I_T are the intensities of the reflected and transmitted radiation, respectively. (b-d) Dependences of the transmitted intensity on the incident radiation intensity. b) Linear regime for an empty resonator. (c) Optical transistor (nonlinear) regime for the nonzero value of the nonlinearity parameter C . (d) Bistability regime for the large value of the nonlinearity parameter C [9]

Its occurrence is determined by the nonlinearity parameter $C = \frac{\alpha L}{2T}$, where α is the absorption coefficient of the medium filling the resonator, L is the length of the resonator and T is the transmissivity of the mirrors. Thus, the operating regimes of the system, depending on the value of this parameter, are illustrated in the Figure 1 b-d).

When we are dealing with an empty resonator, the parameter C equals to zero, so one can only see the linear dependence of the transmitted light on the incident intensity (Figure 1 b). After adding an absorbing medium and, accordingly, increasing the value of C , we begin to observe a nonlinear curve of the transmitted signal depending on the incident radiation in the stationary regime, which is shown in the Figure 1 c). This case corresponds to the optical transistor mode of the system.

Finally, after increasing the parameter C even more, we get an s-curve with a negative slope in the middle. However, the solution, demonstrated by dashed line, is unstable, so the system is describe by the bistable regime (Figure 1 d)). It manifests itself as follows. When we adiabatically increase the intensity of the incident radiation, the system remains in a lower state, and only when the incident intensity reaches the value I_{up} , the transmitted signal undergoes an abrupt transition to a higher branch. In the opposite case, when the value of the incident power decreases, starting to move along the upper branch, the system eventually enters the lower branch after the falling intensity achieves I_{down} . Thus, we see a single cycling of the output signal with an increase and subsequent decrease in the intensity of the incident laser, which leads to a hysteretic behavior of the system.

Moreover, the authors also demonstrate how the fascinating effect of optical bistability can be applied to make the photonic system work as an optical memory element. In fact, the lower and upper states in the input intensity region corresponding to the bistability mode can be used as "0" and "1" units in the optical logic. Namely, by changing the intensity of the incident field, one can pass from one state to another.

Indeed, let us consider a system under continuous irradiation with an incident intensity I_0 . If this structure is initially in the "0" state, then an incoming pulse, illustrated in the Figure 2 b), with a peak intensity above

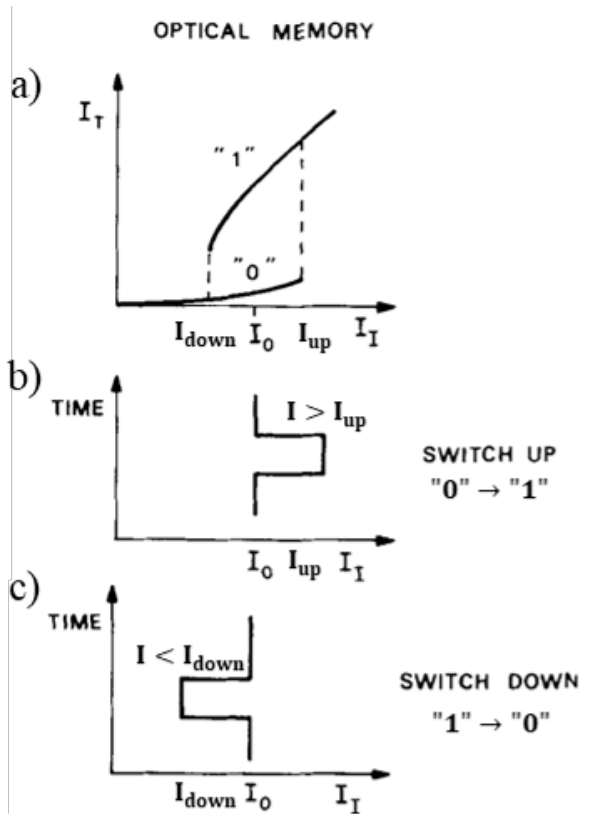


Figure 2 — a) Optical bistability manifested in the dependence of the transmitted signal on the input intensity. b) Switching up the system, constantly irradiated with CW radiation with intensity I_0 and initially occupying the state on the lower branch of the output signal ("0" state) by the pulse with peak intensity $I > I_{up}$. c) Switching down the system, constantly irradiated with CW radiation with intensity I_0 and initially occupying the state on the upper branch of the output signal ("1" state) by the pulse with peak intensity $I > I_{down}$ [9]

$I > I_{up}$ initiates switching to the upper branch and, by the end of the pulse, the system will stay in the upper state, but at the same intensity I_0 (state "1"). At the same time, if the next pulse would come with an intensity below $I < I_{down}$ then the system will switch back to the "0" state (Figure 2 c). Thus, the described process corresponds to the operation of an optical memory based on the optical bistability structure.

Overview of bistable platforms

However, one of the crucial problems preventing the use of such bistable optical systems in real technical applications is their size.

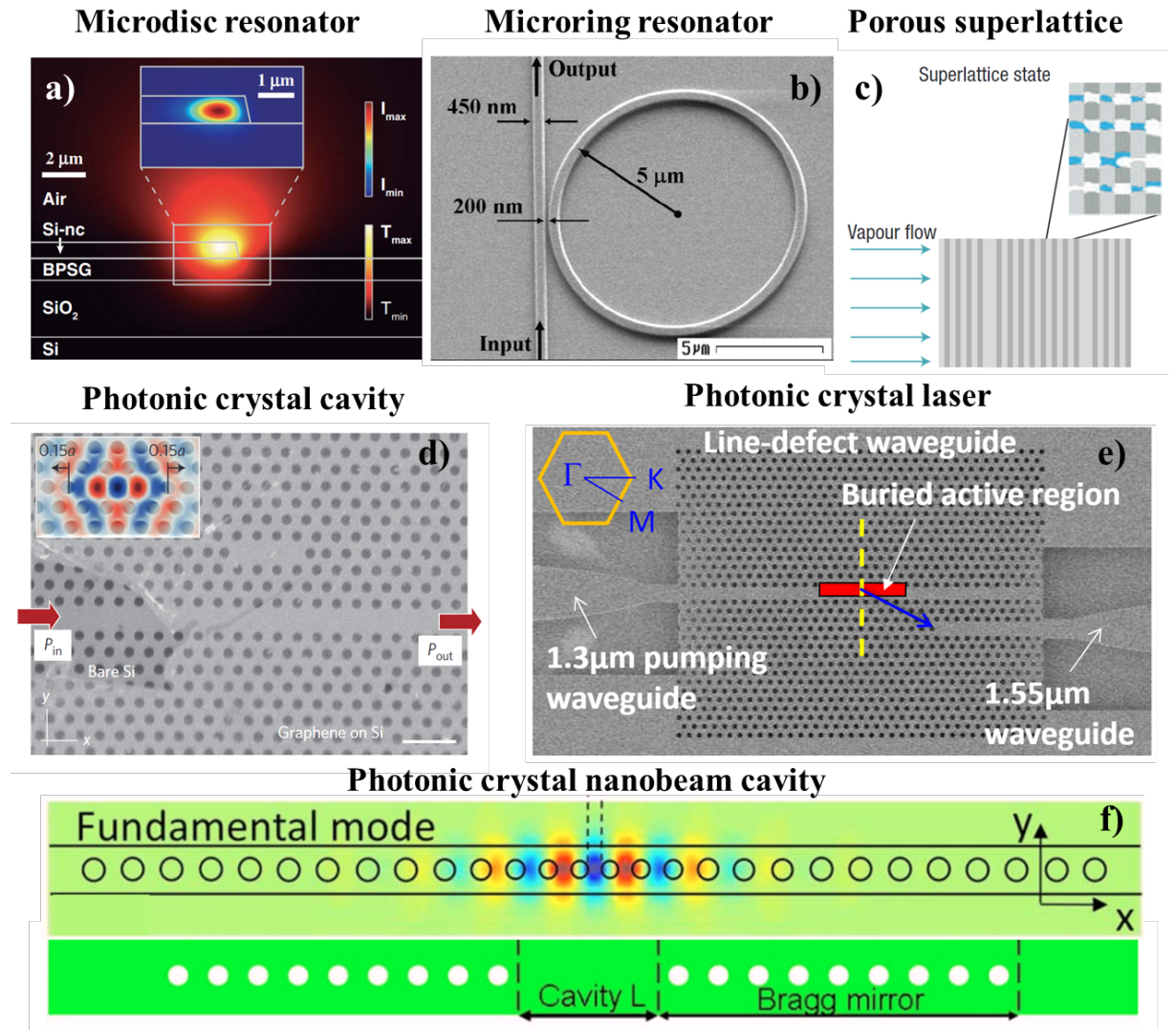


Figure 3 – Various nanophotonic resonance structures exhibiting optical bistability (a) microdisc WGM resonator [10], b) microring resonator [11], c) porous superlattice [12], d) photonic crystal cavity [13], e) photonic crystal laser [14], f) photonic crystal nanobeam cavity [15])

Therefore, following the constant demand for miniaturization of such devices, bistability was sought and observed in various photonic systems, such as microdisk cavities [10], microring resonators [11, 16], photonic crystal cavities [13, 17, 18], photonic crystal waveguides [14] and photonic crystal nanobeam cavities [15]. So, the Figure 3 shows a variety of different microscale resonance platforms in which optical bistability was observed.

For example, in [10] the authors studied the optical bistability in microdisk resonators based on silicon nanocrystals coupled to silicon oxynitride (SiON) waveguides (Figure 4 b)).

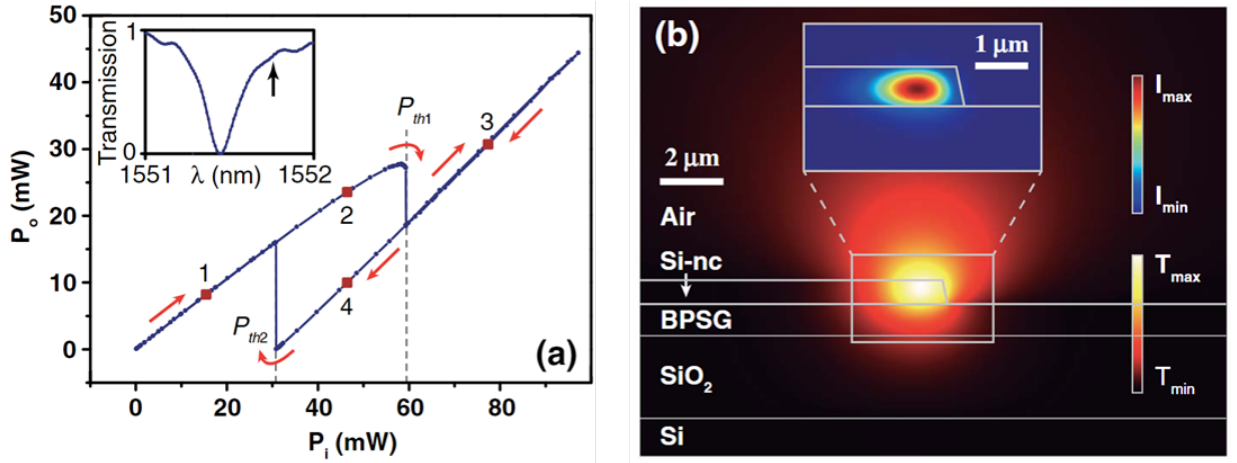


Figure 4 — a) Dependence of transmitted power depending on the incident laser power. The arrow in the inset indicates the position of the pump wavelength relative to the resonant mode. b) Scheme of the microdisk resonator based on silicon nanocrystals with temperature distribution inside this structure. The inset shows the electromagnetic energy density for such calculations [10]

Indeed, the hysteresis behavior of the transmitted incident power as a function of the incident power, obtained in this paper, is shown in the Figure 4 a). In this case, as well as in our work and many other articles [19–21], the optical bistability arises due to the thermo-optical modulation of the refractive index for dielectric materials and the subsequent change in the spectral position of the resonator mode. So, it means that the optical nonlinearity and bistability is related to the dependence of the refractive index on temperature $n(\Delta T)$, which is modulated by the incident laser intensity $\Delta T(I)$. Thus, we are dealing with an intensity-dependent change of the refractive index $\Delta n(I)$ caused by an increase in temperature due to the absorption of radiation. This type of optical bistability is called **thermo-optical bistability**, since it is caused precisely by the heating of the structure.

It should be noted that the change in the refractive index required to observe dispersive optical bistability can be caused by various physical mechanisms. For example, in the work [11] the refractive index decreases due to the free carriers generation based on the two-photon absorption

effect, while in the article [14] optical bistability is observed due to the optical injection locking. Moreover, in [12] the refractive index modulation is associated with capillary condensation, causing the formation of the liquid phase in the porous material.

Finally, along with the thermo-optical mechanism mentioned above, a rather important cause of optical bistability is the Kerr nonlinearity of the medium [13, 17]. However, in most materials, the Kerr effect $n = n_0 + n_2 I$ is very small due to the extremely low non-linearity coefficient n_2 , so really high pump powers are required to modulate the refractive index. At the same time, for most semiconductor materials, there is a pronounced temperature dependence of the refractive index. The latter leads to a strong intensity-dependent thermo-optical modulation of material parameters and may be the crucial mechanism of optical bistability in semiconductor structures. Thus, in [18] authors demonstrate that for silicon structures the thermo-optical mechanism of optical bistability dominates over the Kerr nonlinearity impact due to the very low $n_2 \approx 2.2 \times 10^{-20} \text{ m}^2/\text{W}$ [10] and high $dn/dT \approx 3 \times 10^{-5} \text{ K}^{-1}$ [22] in this optical material.

Thermo-optical effects

Here we would like to deviate a bit from the bistability effect and also recall the importance of various **thermonanophotonics** phenomena that have been actively studied in recent years. Thermal effects in nanophotonics are associated with the ability of nano- and microstructures to absorb electromagnetic radiation incident on them and release heat, which, without clear control and management, can lead to the destruction of nanophotonic structures, but, on the other hand, has many important applications.

Until recently, the field of thermal nano-optics was completely associated with nanoplasmonics. The presence of free electrons in plasmonic structures leads to the appearance of localized surface plasmon resonances [23]. The excitation of these resonances, which significantly enhance optical absorption due to the localization of light near the metal surface, has become the main approach for achieving high efficiency of optical heating in thermonoplasmonics [24–26].

However, the all-dielectric thermonanophotonics has been actively developed recently [27, 28]. Absorption on free carriers, along with single- and multiphoton interband absorption, causes heating of dielectric and semiconductor nano- and microstructures with ohmic losses. The high efficiency of such a process in all-dielectric nanophotonics is connected with the resonant enhancement of light absorption due to the excitation of high-quality optical modes, such as Mie-resonances of a magnetic and electrical nature nanoparticles [29–34] and bound states in the continuum (BIC) or quasi-BIC modes in various nano- and microsystems (single nanocavities [35, 36], one- and two-dimensional arrays of resonant structures or metasurfaces [37–40]).

Moreover, the strong thermo-optical response associated with the temperature dependence of the refractive index of the material [41, 42] has already demonstrated its promise in controlling the linear properties of the radiation for dielectric metasurfaces [43], in modulating nonlinear scattering [44, 45], as well as in tuning such nonlinear processes as second harmonic generation (SHG) [46–49].

However, both in the work mentioned above and in our study, the presence of the temperature-dependent refractive index of the structure material not only allows one to modify and control various properties of the output radiation, but also leads to the appearance of thermo-optical bistability, so that we can observe the output optical signal of different intensities depending on the excitation prehistory at the same conditions.

The aim of work

Finally, due to the rapid development of so-called flat optics, in which classical optical elements are gradually replaced by wavelength-thick metasurfaces and metagratings, optical bistability was also sought in this type of structures [50].

However, this effect has previously been demonstrated only numerically on metal metasurfaces, so **the main goal of this work** was to study thermo-optical bistability in the all-dielectric metasurface structure and develop a theoretical model that would describe such behavior and predict its characteristics.

Our assumption was that the resonant optical heating of the system, enhanced by the high-Q bound state in continuum (BIC) modes, causes a temperature change in the refractive index of the material, resulting in the appearance of spectral resonant shift.

This strong thermo-optical response leads to a self-consistent heating problem and a cubic non-linear equation for the resonator mode energy. Since electromagnetic energy is directly proportional to heating efficiency for quite a broad temperature range [51], then the output thermal state also follows nonlinear dependence. The latter deduction reveals the existence of three possible solutions and, finally, underlies the bistability behavior of optical heating.

In our work, we also investigate various parameters of such thermo-optical hysteresis and derive the conditions for the occurrence of bistability and its observation in experimental setups. In addition, we propose a non-linear critical coupling mechanism that establishes the loss conditions for the maximum hysteresis width.

The reason and advantage of applying the described model specifically to all-dielectric metasurfaces is the ability of such systems to maintain pronounced BIC resonances, leading to strong optical heating and enhancement of thermo-optical nonlinearity, ultimately reaching the bistability regime.

In addition, this structure provides an opportunity to control the parameters of the observed hysteresis loop and switch to the bistability mode by finely controlling the radiative losses during changing the incidence angle of the exciting radiation.

Finally, below we present a comparative table of existing microscale resonant photonic structures in which optical bistability has been observed experimentally. Table 0.1 lists the mechanisms for the appearance of optical bistability, as well as the main resonance and hysteresis characteristics of the structures.

Table 0.1 — Comparison of various resonant photonic microstructures with experimentally observed optical bistability.

Type	Mat.	Mech.	λ_{res} , nm	Q - factor	Size, μm^2	ΔP^{max} / P_{up}	P_{up} , mW	Ref.
Microdisc WGM resonator	Si	Thermo	1552	12500	$50 \times$ 50	0.5	60	[10]
Ring resonator	Si	Free- carriers generation	1533	14000	$10 \times$ 10	0.42	9.5	[11]
Ring resonator	Si	Thermo	1562	14200	$10 \times$ 10	0.39	1.3	[20]
Ring resonator	Si	Thermo	1551	25400	$480 \times$ 65	0.31	0.097	[19]
Point- defect 2D PhC cavity	Graphene /Si	Kerr	1563	7500	\approx 5×5	0.41	0.78	[13]
Hetero- structure PhC laser	InGaAsP /InP	Optical injection locking	1542	100000	\approx $16 \times$ 20	0.33	0.023	[14]
Super- lattice	Porous Si	Capillary conden- sation	973	-	$200 \times$ 200	0.73	12	[12]
BIC Meta- surface	Si	Thermo	950 - 1000	500	$50 \times$ 50	0.3	89	This work

So, from left to right, the columns indicate the type of bistable device, its material, the mechanism of optical bistability, the wavelength λ_{res} and quality factor of the resonant mode, the foot-print size of device, the normalized maximum observed hysteresis width $\Delta P^{max}/P_{up}$, threshold

switching power P_{up} corresponding to the maximum observed hysteresis width and the reference. It includes the articles mentioned earlier and demonstrates the variety and breadth of optical bistability platforms, which can be very promising for various technical applications.

1. MODEL OF OPTICAL HEATING

In this chapter, we would introduce a simplified analytical model for an optical heating based on a single mode resonator approach. By applying coupled mode theory we reveal the principles for nonlinear system response and describe the possible strategies for heating efficiency optimization.

1.1. Single mode resonator model

In general case, optical resonators provide a number of modes which could have overlaps in the spectral region. Moreover, there are a lot of effects based on modes interaction, where transfer of energy from one state to another could occur. However, in most of the cases this interaction is relatively weak and could not be taken into account for heating problems. Besides that, different experimental mechanisms exist which allow to discriminate modes by applying incident radiation with a predefined symmetry profile, like azimuthal vector beams [35] and other higher-order excitation methods. Consequently, we use single mode resonator model which is a good approximation for both describing nonlinear optical heating effect and as an application for bistability in metasurfaces characterization.

1.1.1. Linear resonator model

We started this work from considering the model of a single-mode resonator with a resonant frequency ω_0 and losses γ , which are comprised of radiative γ_r and non-radiative γ_{nr} contributions.

This model can be considered as the simplest analytical model of any high-quality resonant nanostructure, in which, due to the high Q-factor, only one resonant mode can be taken into account [51]. Moreover, it can be well described by the following expression in accordance with the the coupled-mode theory [52]

$$\frac{d\tilde{a}}{dt} = (-i\omega_0 - \gamma)\tilde{a} + i\sqrt{\gamma_r}\tilde{f}, \quad (1)$$

where \tilde{a} - the amplitude of the excited mode in the considered resonator, \tilde{f} - the amplitude of the excitation pump, ω_0 - the eigenfrequency of the resonator, γ and γ_r are the total and radiative losses rates, correspondingly.

In the spectral representation, assuming harmonic excitation and substituting the time dependencies of amplitudes in harmonic form $\tilde{f} =$

$f \exp(-i\omega t)$ and $\tilde{a} = a \exp(-i\omega t)$, we obtain from Equation 1 the following expression for the total energy of the excited mode

$$|a|^2 = \frac{\gamma_r |f|^2}{\gamma^2 + (\omega_0 - \omega)^2} = \frac{\gamma_r |f|^2}{\gamma^2 + \Delta\omega^2}, \quad (2)$$

where $\Delta\omega = \omega_0 - \omega$ is the detuning between the mode eigen-frequency and the frequency of the incident wave.

We introduced here the pump and mode amplitudes so that the total energy excited inside the resonator would be defined as $W = |a|^2$, and the pump power would correspond to $P = |f|^2$.

So, it can be seen that according to the Equation 2, the energy of the mode stored in resonator under continuous wave excitation demonstrates a Lorentzian profile (Figure 1 a)).

1.1.2. Nonlinear resonator model

Now let's introduce a nonlinearity into our system relating to the thermorefractive effect, which takes into account the dependence of the complex refractive index of the material on temperature of the structure $n(\Delta T) + ik(\Delta T)$. A change in the real part of the refractive index $n(\Delta T)$ within the first order of perturbation theory for the single-mode approximation can be considered as an energy dependent shift in the spectral position of the eigenfrequency $\omega_0 \rightarrow \omega_0 - \alpha|a|^2$, while a temperature dependent change in the imaginary refractive index $k(\Delta T)$ entails changes in nonradiative losses $\gamma_{nr} \rightarrow \gamma_{nr} + \beta|a|^2$. This connection will be explained in more detail and derived later in the Subsection 1.1.4.

Thus, in our model, we assume that both loss and resonant frequency vary linearly with mode energy $|a|^2$, and that nonlinear thermo-optical coupling coefficients α and β are positive, which is true for most semiconductor and all-dielectric materials, where both the real and imaginary parts of the refractive index increase with heating [53]. The latter also follows from the exact derivation of the coupling coefficient formulas in Subsection 1.1.4 and means that with increasing temperature, the eigenfrequency of the system shifts to the red region and the ohmic losses increase with the temperature increase. From Figure 1 b) one could see that, as expected, excitation at the so-called 'cold' eigenfrequency ω_0

is no longer optimal which is a consequence of resonance broadening and evolution towards the 'hot' state in spectral range.

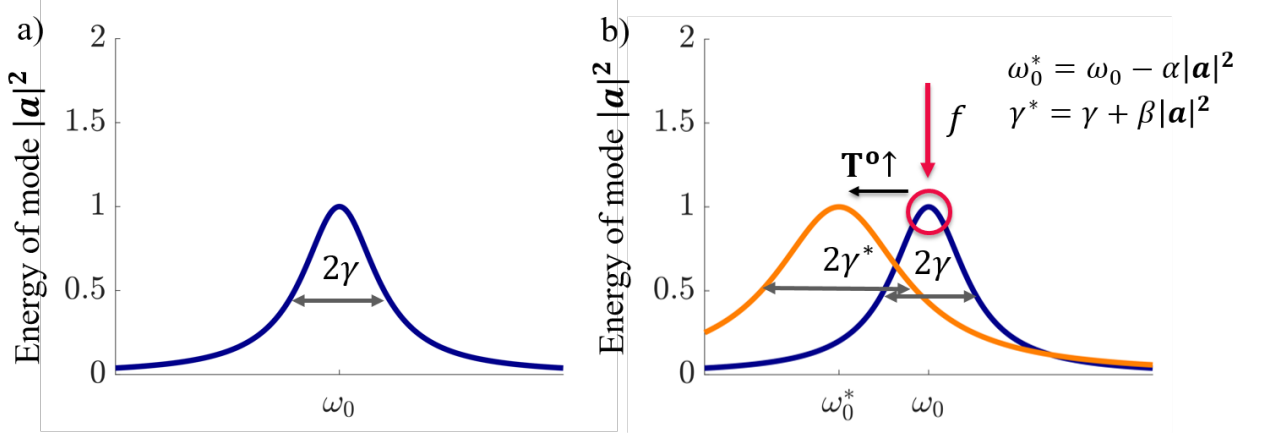


Figure 1 — a) Energy of the mode excited in the single-mode resonator with resonant frequency ω_0 and total losses γ . b) Redshift and resonance broadening of the single-mode resonator due to temperature increase, based on the thermorefractive effect

In order to analyze the perturbed system, we modify the equation for the mode energy. By implementing introduced changes of resonator parameters into initial Equation 2 we obtain the following expression for mode amplitude a :

$$|a|^2 = \frac{\gamma_r |f|^2}{(\gamma + \beta|a|^2)^2 + (\Delta\omega - \alpha|a|^2)^2}. \quad (3)$$

1.1.3. Introduction of dimensionless quantities

In order to analyze the Equation 3, we should introduce dimensionless quantities.

Indeed, let the quantity $y = \alpha|a|^2/\gamma$ be responsible for the mode energy, the pump power will be related to the dimensionless quantity $y_0 = \alpha\gamma_r|f|^2/\gamma^3$, which is the ratio of the mode shift $\alpha|a|^2$ for the zero frequency detuning $\Delta\omega = 0$ in the linear case (Equation 2) to the total losses γ . Moreover, we will also deal with the dimensionless nonlinear thermo-optical coefficient $b = \beta/\alpha$ and the dimensionless frequency detuning $\Delta\tilde{\omega} = \Delta\omega/\gamma$.

Taking into account this introduced quantities, the Equation for the energy of the excited mode 2, obtained in the previous Subsection, turns into the following

$$|a|^2 = \frac{\gamma_r |f|^2}{(\gamma + \beta |a|^2)^2 + (\Delta\omega - \alpha |a|^2)^2} \rightarrow$$

$$y = \frac{y_0}{(1 + by)^2 + (\Delta\tilde{\omega} - y)^2}. \quad (4)$$

Thus, the mode energy y in the system depends only on three independent parameters: the dimensionless pumping power y_0 , the relative nonlinear coefficient b and the dimensionless detuning frequency $\Delta\tilde{\omega}$.

In addition, it can also be noted that for the nonlinear resonator, we obtain a third-degree equation for the mode energy y inside the resonator, leading, under certain parameter settings, to such an interesting effect as thermo-optical bistability, described later in Section 2.

1.1.4. Nonlinear coefficients

In this subsection, we will obtain the exact expressions for the nonlinear coefficients α and β responsible for thermo-optical modulation of the eigenfrequency ω_0 and non-radiative losses γ_{nr} under laser excitation of the system and consequent mode energy $|a|^2$ increase. As it turns out, these coefficients are completely determined by the material parameters of the system (temperature-dependent complex refractive index $n(\Delta T) + ik(\Delta T)$) and the properties of the resonant mode.

Indeed, let's start by considering the previously mentioned thermorefractive effect. With increasing temperature, the refractive index is modified and in the linear approximation can be represented as follows:

$$n(\Delta T) = n_0 + n_1 \Delta T, \quad k(\Delta T) = k_0 + k_1 \Delta T, \quad (5)$$

where n_0 and k_0 - the real and imaginary parts of complex refractive index at room temperature $T = 298\text{K}$, when $n_1 = dn/dT|_{T=298\text{K}}$ and $k_1 = dk/dT|_{T=298\text{K}}$ - the linear coefficients corresponding to the temperature dependencies of the material.

Therefore, based on this description, we can also express the complex permittivity $\varepsilon(\Delta T) = \varepsilon'(\Delta T) + i\varepsilon''(\Delta T)$ as a function of temperature for

both real and imaginary part:

$$\begin{aligned}\varepsilon'(\Delta T) &= \varepsilon'_0 + \varepsilon'_1 \Delta T \approx n_0^2 - k_0^2 + 2(n_0 n_1 - k_0 k_1) \Delta T, \\ \varepsilon''(\Delta T) &= \varepsilon''_0 + \varepsilon''_1 \Delta T \approx 2n_0 k_0 + 2(n_0 k_1 + k_0 n_1) \Delta T,\end{aligned}\quad (6)$$

where we neglected higher terms with respect to temperature increase ΔT in the first order approximation.

On the other hand, optical heating is associated with the conversion of the electromagnetic energy of the incident laser radiation into the thermal energy of the nanostructure. Therefore, the temperature increase ΔT is proportional to the power absorbed by the system:

$$\Delta T = \kappa P_{\text{abs}},$$

where κ is the proportionality coefficient, which depends on the specific geometry of the system and can be found, for example, using accurate numerical modeling.

The absorbed electromagnetic power is defined as

$$P_{\text{abs}} = \frac{1}{2} \text{Re} \int_V \mathbf{J}^*(\mathbf{r}) \mathbf{E}(\mathbf{r}) dV,$$

where $\mathbf{J}(\mathbf{r}) = \sigma \mathbf{E}(\mathbf{r})$ - the complex amplitude of the electric current density. Now we should take into account that the real part of the electrical conductivity $\sigma = \varepsilon_0 \varepsilon'' \omega$, where ε_0 is the vacuum permittivity, ε'' is the imaginary part of the complex permittivity $\varepsilon = \varepsilon' + i\varepsilon''$, ω is the frequency of the incident radiation, $\mathbf{E}(\mathbf{r})$ is the complex amplitude of the electric field and the integral is calculated over the entire volume of the nanostructure. Thus we get

$$P_{\text{abs}} = \frac{\omega}{2} \varepsilon_0 \varepsilon'' \int_V |\mathbf{E}(\mathbf{r})|^2 dV.$$

At the same time, the amplitude of the electric field can be expressed through the introduced earlier excited mode amplitude a as follows

$$\mathbf{E}(\mathbf{r}) = a \mathbf{M}(\mathbf{r}) \sqrt{2} / \sqrt{\varepsilon_0}, \quad (7)$$

where $\mathbf{M}(\mathbf{r})$ is the normalized distribution of the eigenmode field [54]. In general case normalization condition includes integration of the energy over

resonator volume and calculation of corresponding radiative part. However, for high-quality modes, which we are dealing with, radiative losses are significantly suppressed and we can leave only highly confined part for normalization:

$$\int_V \varepsilon'_0 |\mathbf{M}(\mathbf{r})|^2 dV = 1,$$

where ε'_0 is the real part of the complex permittivity at room temperature.

In addition, one can verify that in this case the total energy excited inside the resonator is indeed defined as $W = |a|^2$ after substituting the Equation 7 into the following

$$W = \frac{1}{2} \text{Re} \int_V \mathbf{D}^*(\mathbf{r}) \mathbf{E}(\mathbf{r}) dV = \frac{1}{2} \varepsilon_0 \varepsilon'_0 \int_V |\mathbf{E}(\mathbf{r})|^2 dV.$$

As a result, we can relate the absorbed electromagnetic power P_{abs} or the temperature increase ΔT with the energy of the excited mode $|a|^2$

$$\begin{aligned} P_{\text{abs}} &= \omega \frac{\varepsilon''}{\varepsilon'_0} |a|^2, \\ \Delta T &= \kappa \omega \frac{\varepsilon''}{\varepsilon'_0} |a|^2. \end{aligned} \quad (8)$$

Since in these equations the imaginary part of the permittivity ε'' also depends on the temperature, from the Equation 6 one can obtain the nonlinear relation between the temperature increase and the mode energy:

$$\Delta T = \kappa \omega \frac{\varepsilon''_0}{\varepsilon'_0} |a|^2 + \kappa \omega \frac{\varepsilon''_1}{\varepsilon'_0} \Delta T |a|^2.$$

However, for rather small temperature increases, when $\Delta T \ll \varepsilon''_0/\varepsilon''_1$, the nonlinearity can be neglected, supposing $\varepsilon'' \approx \varepsilon''_0$. We will use this assumption in our derivations.

Moreover, for simplicity of the coefficients expressions we will also assume that the frequency of the incident excitation is in the vicinity of the unperturbed position of the eigenfrequency $\omega \approx \omega_0$.

The eigenfrequency shift is associated with the change in the real refractive index in accordance with the expression:

$$\Delta\omega_0/\omega_0 = -\Delta n/n,$$

where from the introduced mode spectral shift $\Delta\omega_0 = -\alpha|a|^2$ and from Equation 5 $\Delta n = n_1\Delta T$, we can substitute our latter derivation in this expression and get the nonlinear coefficient α

$$\alpha = \frac{\omega_0 n_1 \Delta T}{n_0 |a|^2} \approx \frac{\kappa \omega_0^2 n_1 \varepsilon_0''}{n_0 \varepsilon_0'} = \frac{2\kappa \omega_0^2 n_1 k_0}{n_0^2 - k_0^2},$$

where all material parameters correspond to the eigenfrequency ω_0 due to the assumption $\omega \approx \omega_0$.

On the other hand, from the definition of the amplitude nonradiative losses and the Equation 8

$$\gamma_{\text{nr}} = \frac{P_{\text{abs}}}{2|a|^2} = \frac{\omega \varepsilon_0''}{2 \varepsilon_0'} + \frac{\omega \varepsilon_1''}{2 \varepsilon_0'} \Delta T. \quad (9)$$

Therefore, recalling the introduced change of non-radiative losses $\Delta\gamma_{\text{nr}} = \beta|a|^2$, we finally can obtain the nonlinear coefficient β

$$\beta = \frac{\omega \varepsilon_1'' \Delta T}{2 \varepsilon_0' |a|^2} \approx \frac{\kappa \omega_0^2 \varepsilon_1'' \varepsilon_0''}{4 \varepsilon_0'^2} = \frac{\kappa \omega_0^2 n_0 k_0 (n_0 k_1 + n_1 k_0)}{(n_0^2 - k_0^2)^2}.$$

Finally, we can express the dimensionless nonlinear thermo-optical parameter b and note that it is determined only by the characteristics of the material and does not depend on the resonant properties of the system:

$$b = \frac{\beta}{\alpha} = \frac{n_0 (n_0 k_1 + n_1 k_0)}{2 n_1 (n_0^2 - k_0^2)}. \quad (10)$$

1.2. Optimal heating condition

The optimization problem of the nanostructure heating is one of the interesting problems that can be solved on the basis of the described single-mode resonator model. In the linear regime, the solution maximizing the temperature increase of the nanostructure is well known and is called critical coupling condition [55].

In this section, we present a simple derivation of this expression in the linear case, and also generalize it to the nonlinear regime, when the thermorefractive effect is taken into account in the system.

1.2.1. Linear critical coupling

Indeed, returning to the Equations 2, 9, we find that the temperature rise proportional to the absorbed electromagnetic power and in the linear

case can be described by the simple Lorentzian profile:

$$\Delta T \sim P_{\text{abs}} = \frac{2\gamma_{nr}\gamma_r|f|^2}{(\gamma_{nr} + \gamma_r)^2 + \Delta\omega^2},$$

where $\Delta\omega = \omega_0 - \omega$. The maximum of this frequency function is reached at the point $\omega = \omega_0$. In addition, having fixed the value of radiative losses, we find that the optimal coupling is achieved when radiative and ohmic losses are balanced with each other $\gamma_{nr} = \gamma_r$. The last expression identifies the critical coupling condition for optimal heating in the linear regime.

1.2.2. Nonlinear critical coupling

When we are dealing with a non-linear case and assume the presence of a non-zero nonlinear coefficients α and β , it is quite useful to move from the Equation 4 to a more compact normalized form

$$y = \frac{y_{\text{max}}}{1 + (y - y_{sh})^2/\Gamma^2}, \quad \text{where}$$

$$y_{\text{max}} = \frac{y_0(b^2 + 1)}{(b\Delta\tilde{\omega} + 1)^2}, \quad y_{sh} = \frac{\Delta\tilde{\omega} - b}{1 + b^2}, \quad \Gamma = \frac{1 + b\Delta\tilde{\omega}}{1 + b^2}.$$

This expression implies the assertion that the excited energy inside the resonator cannot exceed the value of y_{max} . Moreover, it reaches this maximum when the condition $y = y_{sh}$ is fulfilled. By combining these two conclusions we come to the following expression on electromagnetic energy maximization, which we refer to as critical coupling line in parametric space of detuning and incident intensity $\Delta\tilde{\omega} - y_0$:

$$(\Delta\tilde{\omega} - b)(b\Delta\tilde{\omega} + 1)^2 = y_0(b^2 + 1)^2. \quad (11)$$

One could see from this equation, that in contrast to the linear case, the optimal detuning $\Delta\omega = \Delta\tilde{\omega} \cdot \gamma$ is now defined by incoming power y_0 . This conclusion is logical in a sense that the more incident excitation we apply to our system, the bigger the shift of the resonant peak occurs and the larger incident detuning between laser and resonant mode should be used for heating optimization.

One important case corresponds to the situation of zero thermo-optical parameter b , when losses do not change with increasing temperature. This case could correspond to near-IR excitation when change of the bandgap is

still not sufficient to increase absorption rate. From Equation 11 we obtain then that

$$\Delta\tilde{\omega} = y_0,$$

or, by introducing initial definitions

$$\Delta\omega = \frac{\alpha\gamma_r}{\gamma^2}|f|^2,$$

which means that the maximum possible value of optical heating is achieved when frequency detuning is directly proportional to the pump power.

Furthermore, we recall the definition of introduced dimensionless quantities which are $y_0 = \alpha\gamma_r|f|^2/\gamma^3$ and $y = \alpha|a|^2/\gamma$. Therefore, we can also rewrite expression on mode energy maximization

$$y = y_{\max} = \frac{y_0(b^2 + 1)}{(b\Delta\tilde{\omega} + 1)^2},$$

as follows

$$|a|^2 = \frac{\gamma_r|f|^2(b^2 + 1)}{\gamma^2(b\Delta\tilde{\omega} + 1)^2} = \frac{\gamma_r|f|^2(b^2 + 1)}{(b\Delta\omega + \gamma)^2}.$$

As a result, substituting the energy of the excited mode into the Equation 9, we see that heating in the optimized mode $y = y_{\max}$ has an expression similar to the linear case, but not the same

$$\Delta T \sim P_{\text{abs}} = \frac{2\gamma_{nr}\gamma_r|f|^2(1 + b^2)}{(\gamma_r + \gamma_{nr} + b\Delta\omega)^2}. \quad (12)$$

Therefore, with thermo-optical nonlinearity, the maximum heating efficiency is achieved under conditions different from the linear case. Having fixed the value of radiative losses, it can be obtained from the Equation 12 that the non-radiative losses in the system must be detuned from radiative losses:

$$\gamma_r = \gamma_{nr} + b\Delta\omega.$$

Finally, the last equation is the generalization of the critical coupling condition for optimal heating in the nonlinear case.

2. THERMO-OPTICAL BISTABILITY

2.1. Bistability effect

Let us consider in more detail the equation for the excited mode energy, obtained in the nonlinear case of the thermo-refractive effect in terms of dimensionless quantities:

$$y = \frac{y_{\max}}{1 + (y - y_{sh})^2/\Gamma^2}, \quad \text{where}$$

$$y_{\max} = \frac{y_0(b^2 + 1)}{(b\Delta\tilde{\omega} + 1)^2}, \quad y_{sh} = \frac{\Delta\tilde{\omega} - b}{1 + b^2}, \quad \Gamma = \frac{1 + b\Delta\tilde{\omega}}{1 + b^2}.$$

As mentioned in the subsection 1.1.3, this expression is a nonlinear cubic equation for the mode energy inside the resonator y .

So, depending on the initial parameters, this expression can have one, two or three solutions. The latter case corresponds to the appearance of bistability. The region of pump parameters corresponding to this effect is called the hysteresis region, where the solution of the equation is described by an s-shaped curve (Figure 1).

However, in real physical systems, the solution in the middle, indicated by the dotted line, is unstable, and the system falls into one of two stable states, upper (hot) or lower (cold), depending on the excitation pre-history.

Since from the Equation 8 the temperature increase ΔT in the system is proportional to the mode energy $|a|^2$, we can also claim that the hysteresis behavior manifests itself not only in the mode energy accumulated in the system $|a|^2$ (or y), but also in its temperature T .

In experiment, as it was mentioned in the Introduction, the described effect is usually observed in the following way. With a gradual increases in the falling pumping power, the mode energy, and consequently the temperature, gradually increase, following along the lower branch up to the edge point B of the hysteresis region. With a further increase in laser power, the only possible solution turns out to be on the upper branch, so there is a sharp jump in temperature. During the reverse pass in pumping power, when the resonator is already in a hot state, the system begins to move along the upper branch in the opposite direction until it reaches

the leftmost point of hysteresis A and again falls onto the lower branch. Thus, it turns out that the system behaves differently when increasing and decreasing the falling pumping power.

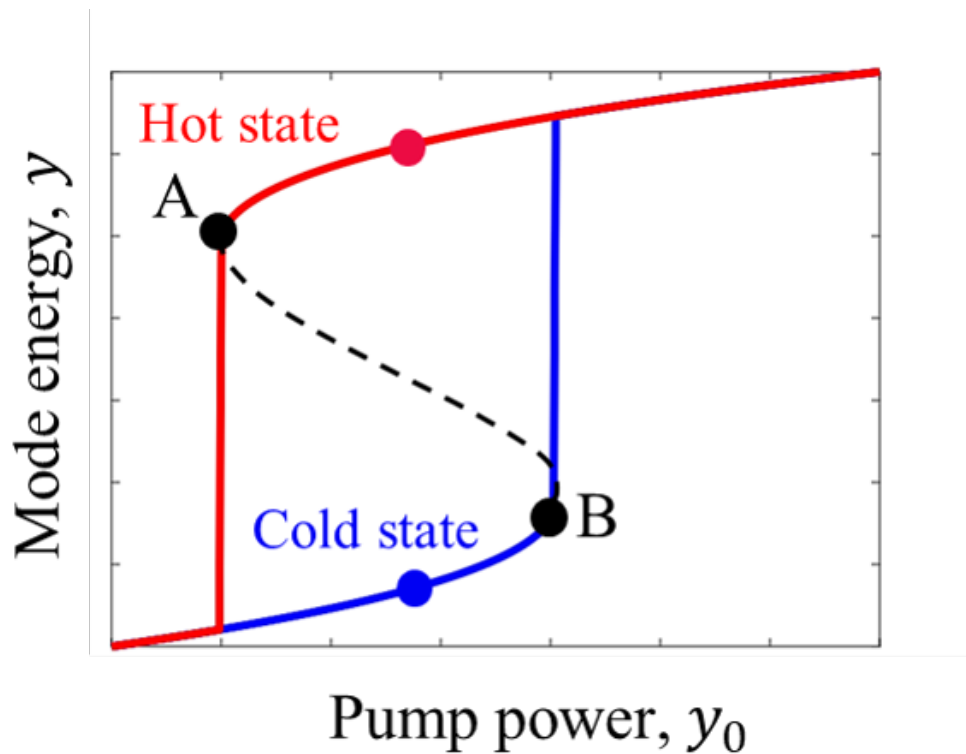


Figure 1 — Hysteresis loop in the dimensionless axes (pump power y_0 - mode energy y). The blue line corresponds to the increasing sequence of falling laser power, and the red line to the decreasing sequence. Black points A and B are the turning points of the hysteresis curve. The dotted line marks the unstable solution

Thus, **thermo-optical bistability** is a temperature-induced regime of an optical system, manifested by a hysteresis response, when the system is able to be in a "hot" and "cold" state under the same excitation conditions determined by the prehistory of excitation.

2.2. Bistability condition

As mentioned earlier, achieving a bistability regime in a system is not always possible and depends on the parameters of the system and excitation. So, in this section, based on a detailed analysis of the positions of the

edge (turning) points A and B, we derive the bistability condition for the nonlinear system.

To begin with, let's rewrite the third-degree nonlinear equation for the dimensionless excited mode energy in the function form

$$\begin{aligned} f &= y \cdot \left[\Gamma^2 + (y - y_{sh})^2 \right], \\ f(y) &= \frac{y_0}{1 + b^2}. \end{aligned} \quad (1)$$

Introduced function f is cubic with respect to energy y and we need to find the conditions for which the equation $f(y) = const$ has exactly two solutions. This case corresponds to the edges of hysteresis area, as one could see from Figure 1. Thus, by taking the derivative of this function with respect to y and equating it to 0, one can obtain the values of the excited mode energy corresponding to the turning hysteresis points

$$\begin{aligned} y_A &= \frac{1}{3} \left(2y_{sh} + \sqrt{D} \right), \\ y_B &= \frac{1}{3} \left(2y_{sh} - \sqrt{D} \right), \\ D &= y_{sh}^2 - 3\Gamma^2. \end{aligned} \quad (2)$$

From this expression it becomes clear that the bistability effect occurs only when the value of the parameter D is greater than zero, since the existence of turning points is possible in this case.

Substituting the values of the excited mode energy from the Equation 2 into the function $f(y)$ in the Equation 1, we also obtain the dimensionless pump power corresponding to the edge points A and B

$$\begin{aligned} y_0(A) &= f(y_A) \cdot (1 + b^2) = \frac{2}{27} \left(y_{sh} \cdot [y_{sh}^2 + 9\Gamma^2] + D^{3/2} \right) \cdot (1 + b^2), \\ y_0(B) &= f(y_B) \cdot (1 + b^2) = \frac{2}{27} \left(y_{sh} \cdot [y_{sh}^2 + 9\Gamma^2] - D^{3/2} \right) \cdot (1 + b^2). \end{aligned} \quad (3)$$

Now recalling the expressions for y_{sh} and Γ , we can also derive the bistability condition in terms of the dimensionless frequency detuning $\Delta\tilde{\omega}$ and the nonlinear thermo-optical parameter b

$$\begin{aligned} D &> 0, \\ (\Delta\tilde{\omega} - b)^2 &> 3(b\Delta\tilde{\omega} + 1)^2. \end{aligned} \quad (4)$$

When analyzing the bistability condition and taking into account that the incident dimensionless power y_0 from the Equation 3, which corresponds to the two branches of the hysteresis, must be positive, there is some restriction on the non-linear coefficient β . It turns out that this parameter cannot exceed a certain critical value $b < b_{cr} = 1/\sqrt{3}$, so that the bistability is implemented in the system. This is due to the fact that the bistability condition for $b > 1/\sqrt{3}$ is satisfied only for negative, and hence non-physical values of the incident power y_0 . In fact, one could interpret this condition in following way: since relative coefficient b is defined by the ratio of losses β versus eigenmode frequency α thermo-optical shift factors, then for the large values of losses shifts, meanwhile $\beta > \alpha/\sqrt{3}$, width of the resonance grows faster with increasing temperature than the eigenmode position changes. This behaviour limits the possibility of the system to noncontinuously change its state.

Moreover, by considering the positiveness of y_0 , one can also obtain that for systems in which the resonance broadening with increasing temperature is much less than the resonance frequency shift, i.e. $b = \beta/\alpha \approx 0$, the bistability condition 4 is greatly simplified and takes the following form

$$\Delta\tilde{\omega} > \sqrt{3}. \quad (5)$$

Indeed, for a zero dimensionless nonlinear coefficient b , Figure 2 b) shows that in the case of a dimensionless frequency detuning less than $\sqrt{3}$, only a strong nonlinear response of the system can be observed (blue line). Otherwise, when $\Delta\omega/\gamma = 3 > \sqrt{3}$, the bistability mode is achievable, which is indicated in red.

2.3. Hysteresis parameters

So, in the previous section we deduced the condition when bistability is realized in our nonlinear system. In this section, we will introduce and analyze such crucial from an experimental point of view characteristics of our hysteresis loop as its height H_h and width W_h (Figure 2 a)). The width of the hysteresis W_h or the distance between the turning points A and B along the pump power axis characterizes the sensitivity of switching the excited mode energy or temperature during changing the incident pumping. At the

same time, the height H_h or the distance between A and B points relative to the y axis shows the temperature change between the two states (warm and cold, respectively).

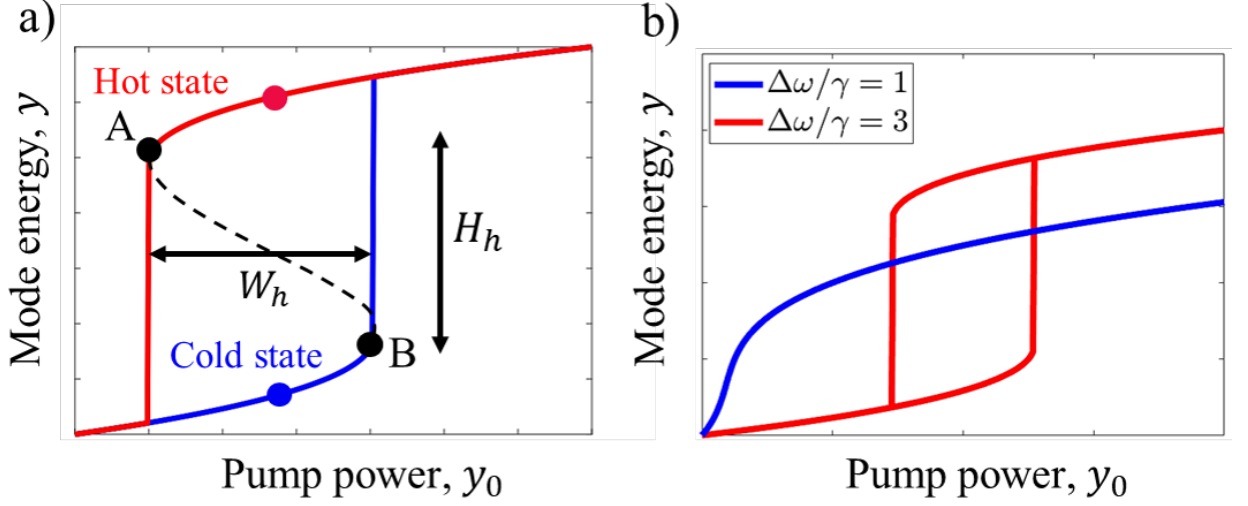


Figure 2 — a) Hysteresis loop in dimensionless axes (pump power y_0 - mode energy y) with the mark of its main characteristics (height H_h and width W_h). b) Solution modes for the excited mode energy depending on the dimensionless frequency detuning. The blue line shows the case when the bistability condition is not satisfied $\Delta\omega/\gamma = 1 < \sqrt{3}$ and the system has only a strong nonlinearity, while in the second case (red loop) the system possesses bistability $\Delta\omega/\gamma = 3 > \sqrt{3}$

Hysteresis width W_h is an important parameter to be optimized since nonlinear elements of optical logic should be resistant to incoming noise while still be achievable within the incoming signal modulation. If the width of bistability area is comparable to the noise level than signal fluctuations could switch the system from one state to another and produce data misinterpretation. On the other hand, for large width of hysteresis loop one should apply high amplitude of signals modulation which slows down the overall speed of device operation and leads to higher energy consuming.

Using the Equation 2, one can immediately find the dimensionless height of the hysteresis region

$$H_h = y_A - y_B = \frac{2\sqrt{D}}{3}.$$

In addition, by subtracting one expression of the Equations 3 from another, we also simply determine the width of the hysteresis region:

$$W_h = y_0(B) - y_0(A) = \frac{4D^{3/2}}{27} \cdot (1 + b^2) = H_h^3 \frac{1 + b^2}{2}.$$

Here it is worth noting that from the form of obtained formulas for the height and width of the hysteresis, the condition for the bistability existence $D > 0$ becomes obvious. Indeed, if it is not fulfilled or when $D \rightarrow 0$, the hysteresis collapses and the height and width are reset to zero.

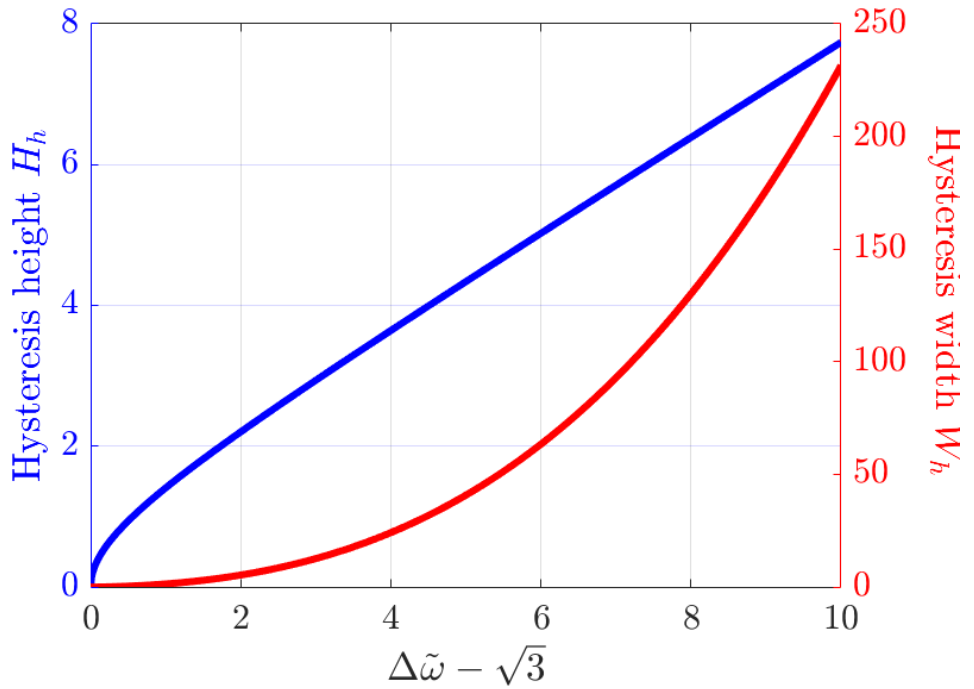


Figure 3 — Hysteresis parameters depending on the dimensionless frequency detuning. The red line refers to the width of the hysteresis, the blue line corresponds to the height of the hysteresis loop

In the previously mentioned case, when the non-linear thermo-optical coefficient b is approximately equal to 0, the expressions for the hysteresis parameters take an even simpler form and depend only on the dimensionless frequency detuning $\Delta\tilde{\omega}$:

$$H_h = \frac{2}{3} \sqrt{\Delta\tilde{\omega}^2 - 3},$$

$$W_h = \frac{H_h^3}{2}.$$

The Figure 3 depicts the dependence of the dimensionless hysteresis width W_h and height H_h on the dimensionless frequency detuning $\Delta\tilde{\omega}$ for zero thermo-optical non-linear coefficient b .

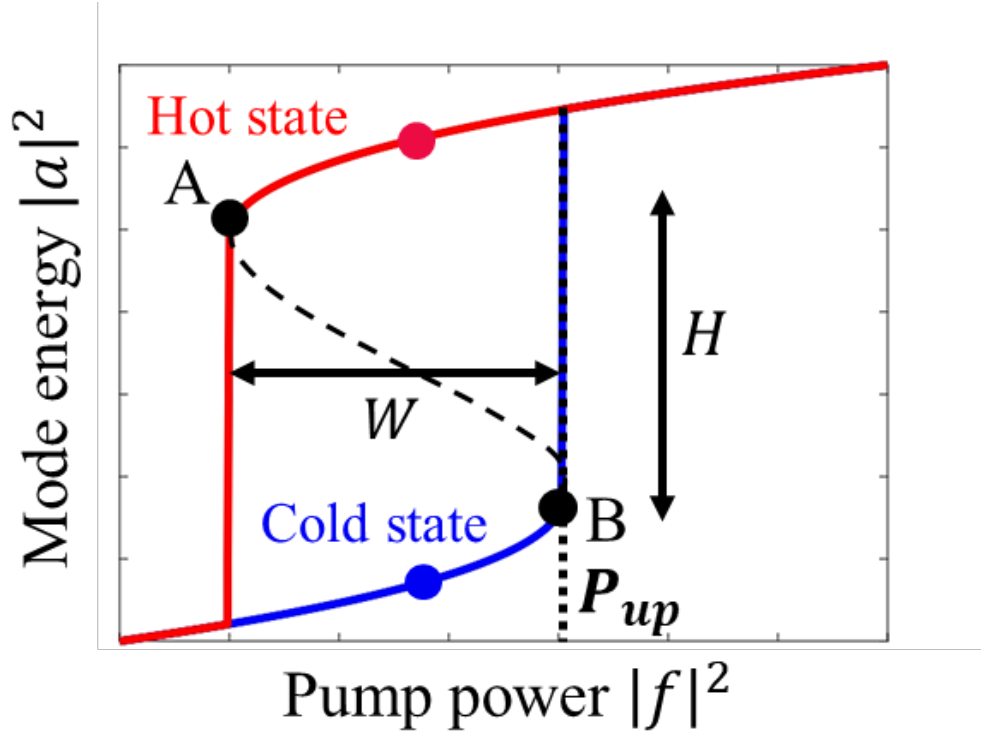


Figure 4 — Hysteresis loop in dimensional axes (pump power $|f|^2$ - mode energy $|a|^2$) with the mark of its main characteristics (height H_h , width W_h and the switching power from the cold to the hot state of the system P_{up})

It can be noted that for sufficiently large detunings, the height of the hysteresis is proportional to the frequency detuning $H_h \sim \Delta\tilde{\omega}$, while the hysteresis width is related to the latter in a cubic way $W_h \sim \Delta\tilde{\omega}^3$. If the frequency of the incident pumping is in close proximity to the boundary of bistability condition 5, which means that $\Delta\tilde{\omega} = \sqrt{3} + \tilde{\Delta}$, then the height will depend on this small value $\tilde{\Delta}$ in a root way $H_h \sim \tilde{\Delta}^{1/2}$, and the width as $W_h \sim \tilde{\Delta}^{3/2}$.

In experimental problems, we often deal with the dimensional values of the excited mode energy and the incident power. Therefore, it is also necessary to express the dimensional parameters of the hysteresis. In order to do this, we should recall the relationship between dimensional and

dimensionless characteristics from the Subsection 1.1.3 and finally obtain the following expressions (Figure 4)

$$\begin{aligned}
 H &= \frac{\gamma H_h}{\alpha} = \frac{2\gamma}{3\alpha} \left(\frac{\Delta\omega^2}{\gamma^2} - 3 \right)^{1/2}, \\
 W &= \frac{\gamma^3 W_h}{\alpha\gamma_r} = \frac{4}{27} \frac{\gamma^3}{\alpha\gamma_r} \left(\frac{\Delta\omega^2}{\gamma^2} - 3 \right)^{3/2}.
 \end{aligned} \tag{6}$$

3. BISTABILITY EXISTENCE AREA AND CRITICAL COUPLING CONDITION

In this section we will focus on more detailed description of thermo-optical hysteresis appearance in real physical systems. We would discuss constrains applied for the experimental realisation of bistability behaviour and provide discussion on the case of limited excitation power. Moreover, we provide analytical description for hysteresis width maximization and the ways for its experimental realisation.

3.1. Bistability existence area

In section 2.2 we derived conditions for the dimensionless frequency detuning $\Delta\tilde{\omega}$ and the nonlinear thermo-optical parameter b to implement thermo-optical bistability in the system.

Hence, it can be assumed that, in principle, any nonlinear resonator with $b < b_{cr} = 1/\sqrt{3}$ can be transferred to the bistable regime by adjusting frequency detuning. However, this is correct only in an ideal theoretical study, when we are able to arbitrarily tune the excitation parameters so as to achieve bistability appearance condition and turn the system to the hysteretic output mode, whereas in experimental applications we always deal with some limitations.

One of such limitations is limited pumping power, which underlies the power restriction in our model

$$P < P_{max},$$

where P_{max} is the maximum possible excitation power available in the experimental setup.

Indeed, let's consider the laser power that should be set for the experimental observation of bistability in the structure. It corresponds to the switching power from the cold to the hot state of the system P_{up} and refers to the boundary point B for hysteresis loop in dimensional axes (Figure 4).

The equation for this quantity can be expressed by adding the dimension factor in the dimensionless Equations 3 as follows

$$\begin{aligned}
P_{up} &= \frac{2}{27} \frac{\gamma^3}{\alpha\gamma_r} \left(\frac{\Delta\omega}{\gamma} \left[\frac{\Delta\omega^2}{\gamma^2} + 9 \right] \right) + \frac{W}{2} = \\
&= \frac{2}{27} \frac{\gamma^3}{\alpha\gamma_r} \left(\frac{\Delta\omega}{\gamma} \left[\frac{\Delta\omega^2}{\gamma^2} + 9 \right] \right) + \frac{2}{27} \frac{\gamma^3}{\alpha\gamma_r} \left(\frac{\Delta\omega^2}{\gamma^2} - 3 \right)^{3/2}.
\end{aligned} \tag{1}$$

Thus, in the Figure 1 one can see the region of bistability realization, demonstrated by black lines. It turns out that under laser power limitation the hysteresis region is confined not only from below by the condition for the bistability occurrence $\Delta\omega/\gamma > \sqrt{3}$ (red dashed line), but also from above by the power restriction line $P_{up} < P_{max}$ (blue solid line).

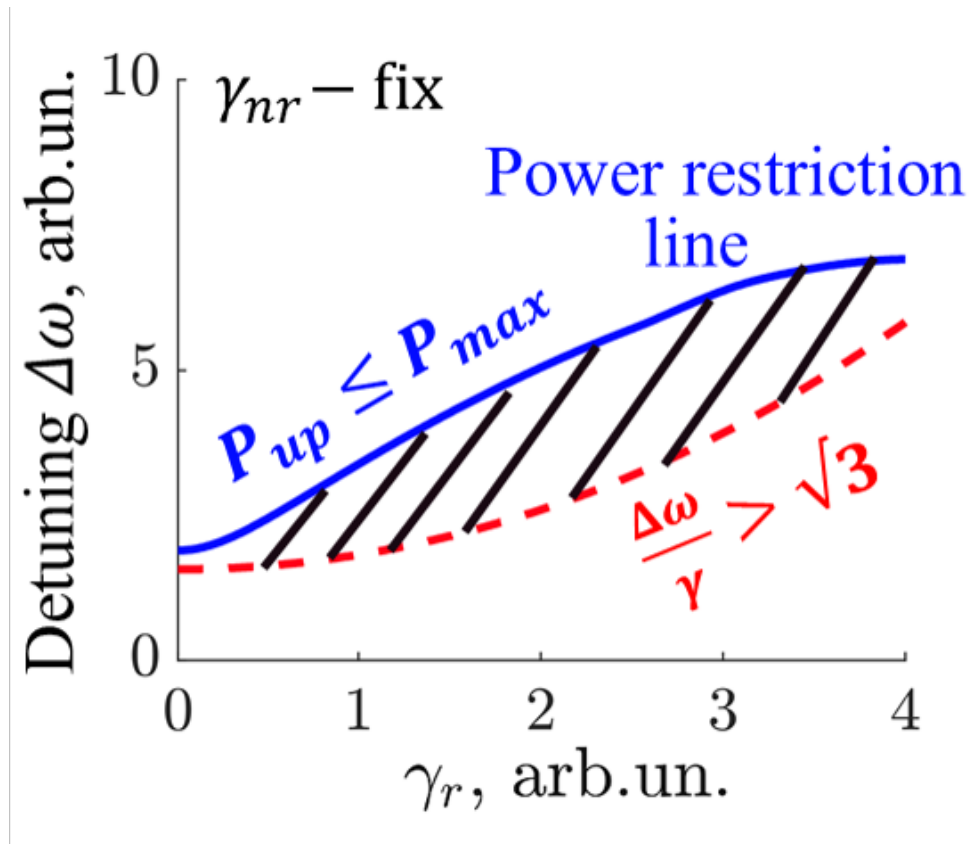


Figure 1 — Area of hysteresis existence depending on radiative losses and frequency detuning for the case of fixed non-radiative losses. The upper boundary red line corresponds to the power restriction, and the lower one refers to the bistability condition

3.2. Efficient reaching of bistability regime

In this section, we analyze and present the critical coupling condition for the balance between radiative and nonradiative losses of the system,

which provides the lowest necessary pump power to achieve the bistability regime.

We will work under the assumption that the non-linear thermo-optical parameter is approximately zero and use the simple form of the bistability condition (Equation 5) $\Delta\omega/\gamma > \sqrt{3}$.

Let us return to the switching power P_{up} and substitute the boundary of bistability condition into the Equation 1

$$P_{up}(\Delta\omega/\gamma = \sqrt{3}) = \frac{8\sqrt{3}}{9} \frac{\gamma^3}{\alpha\gamma_r} = P_{cr}.$$

Thus, it turns out that even if we managed to tune the system parameters in such a way that the bistability regime could be achieved, we also always have to set P_{max} not lower than the critical value P_{cr} in order to observe the bistability of the system in the experiment.

Let us consider in more detail the obtained critical value of the pump power for achieving the bistability regime

$$P_{cr} = \frac{8\sqrt{3}}{9} \frac{\gamma^3}{\alpha\gamma_r}$$

By taking the derivative of P_{cr} , one can see that for fixed nonradiative losses, the loss function reaches a minimum when the radiative losses are half the nonradiative:

$$\gamma_{nr} = 2\gamma_r.$$

Thus, this loss condition refers to the most efficient way of reaching bistability when we are dealing with limited pumping, since it minimizes the critical power required to observe the hysteretic behavior of the system.

Finally, it is worth noting that the minimization of laser power required for bistability is so important because of the reduction in power consumption, which is the most overspread problem in many experimental applications.

3.3. Maximization of hysteresis width

From another point of view, in order to apply thermo-optical bistability to optical elements and ensure their resistance to the noise of incoming signals and careful switching between upper and lower states, we

are interested in maximizing the width of the hysteresis loop, which cannot grow infinitely in the case of power limitation $P < P_{max}$.

Let's go back to the dimensional Equation 6 of this hysteresis parameter

$$W = \frac{4}{27} \frac{\gamma^3}{\alpha \gamma_r} \left(\frac{\Delta\omega^2}{\gamma^2} - 3 \right)^{3/2}. \quad (2)$$

First of all, it can be noted that as the detuning frequency increases, the width of the dimensional hysteresis, as well as the switching power P_{up} , limited from above by the maximum allowable laser power P_{max} , simultaneously rise.

Therefore, we have to impose the condition $P_{up} = P_{max}$ and solve the conditional maximum problem on the width of the hysteresis loop. We need to notice that as soon as power restriction condition is applied to our system, frequency detuning $\Delta\omega_{max}$ is no longer an independent parameter and should be derived from $P_{up} = P_{max}$ equation for every value of the losses rate. By applying given above considerations and recalling the definition of the switch power in dimensional parameters we come to following optimization problem:

$$\frac{2}{27\alpha} \frac{\gamma^3}{\gamma_r} \underbrace{\left(\frac{\Delta\omega_{max}}{\gamma} \left[\frac{\Delta\omega_{max}^2}{\gamma^2} + 9 \right] \right)}_{\text{term to minimize}} = \left(P_{max} - \frac{W_h}{2} \right), \quad (3)$$

where term on the left side should be minimized with respect to radiative losses γ_r (we fix nonradiative part γ_{nr}) for width maximization and $\Delta\omega_{max}$ is an implicit function of losses defined by maximum power condition. Thus, one can simply take the derivative of the left optimization term, for example, with respect to radiation losses γ_r , and set it to zero.

However, the most tricky part of optimization is defining the derivative of the maximum detuning $d\Delta\omega_{max}/d\gamma_r$. For this purpose we utilize the following equation:

$$\frac{1}{\gamma_r} \left[\Delta\omega_{max}^3 + 9\gamma^2 \Delta\omega_{max} + (\Delta\omega_{max}^2 - 3\gamma^2)^{3/2} \right] - C = 0, \quad (4)$$

which is a direct transform of Equation 1 with $P_{up} = P_{max}$ condition and where $C = 27\alpha P_{max}/2$. Taking the derivative of this equation over radiative

losses and taking into account that $d/d\gamma = d/d\gamma_r$, since $\gamma = \gamma_r + \gamma_{nr}$ and nonradiative losses are fixed we come to following expression for the derivative we are interested in:

$$\frac{d\Delta\omega_{max}}{d\gamma_r} = \frac{C - 18\gamma\Delta\omega_{max} + 9\gamma(\Delta\omega_{max}^2 - 3\gamma^2)^{1/2}}{3(\Delta\omega_{max}^2 + 3\gamma^2 + \Delta\omega_{max}(\Delta\omega_{max}^2 - 3\gamma^2)^{1/2})}. \quad (5)$$

So, finally, by substituting this derivative into the total derivative of the optimization term mentioned above and equating the latter to zero, we finally can solve the conditional maximum problem and find that the maximum hysteresis width W is reached at nonradiative losses twice as large as radiative ones (Figure 2), which is the same losses ratio condition as for the effective achievement of the bistability regime, obtained in Section 3.2.

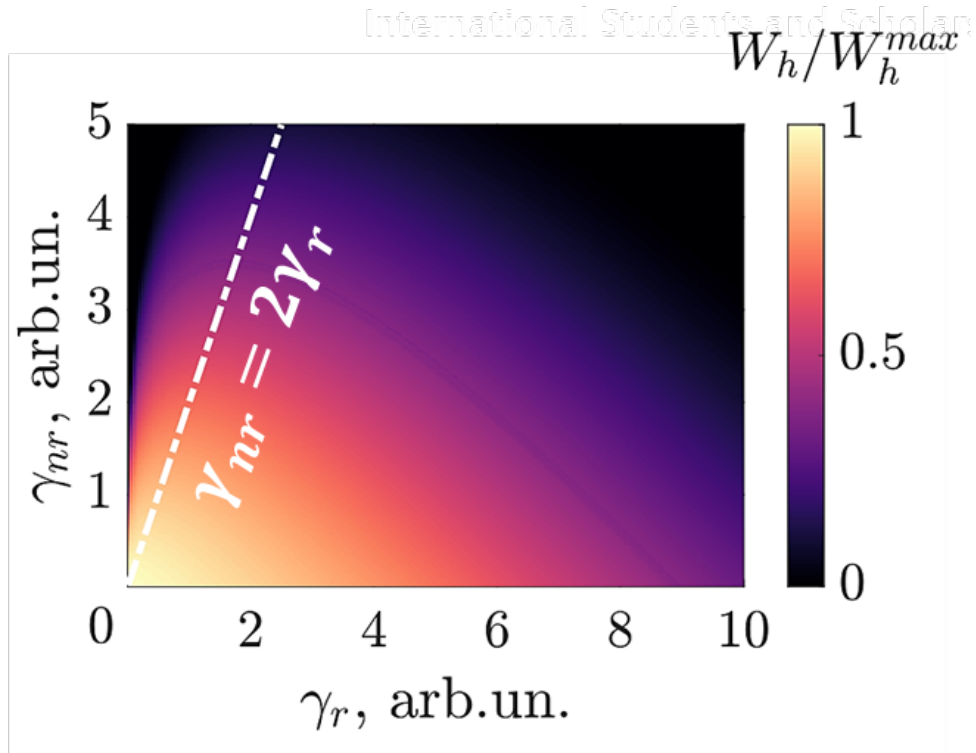


Figure 2 — Map of the calculated hysteresis width depending on the radiative and nonradiative losses under the condition $P_{up} = P_{max}$. The white line indicates the critical coupling condition for the loss that maximizes the width of the hysteresis loop

As a result, we called $\gamma_{nr} = 2\gamma_r$ the nonlinear critical coupling condition and claim that it characterizes the maximum possible hysteresis

width at a fixed threshold laser power P_{max} and corresponds to the most efficient reaching of the bistability in the system.

As stated above, given ratio is exactly the same as was discussed for the critical power minimization. That is a logical conclusion in a sense that for fixed maximum pump value the lowest power for bistability appearance provides the broadest range for detuning variations. Therefore, these two approaches give us exactly the same answer.

4. BISTABILITY IN METASURFACES

In this section we apply our analytical analysis towards experimental data on bistability acquisition in two-dimensional semiconductor membrane. The experiment was carried out by Alexander Barulin and Alexander Chernov at the Moscow Institute of Physics and Technology. We prove the correspondence between theoretical dependence of hysteresis width on losses rate with real physical system behaviour. Moreover, we emphasize critical coupling condition realized for a quasi-BIC mode in a membrane and determine incident values required for its achievement.

4.1. Quasi-BIC mode

Finally, in this work we apply our developed theoretical model of nonlinear resonator for the description of optical bistability experimentally observed by colleagues on the perforated silicon metasurface membrane, demonstrated on the Figure 1 a). The described system has a size of $50 \mu\text{m}^2 \times 50 \mu\text{m}^2$ and consists of periodically spaced slightly conical holes with an upper diameter of about 310 nm. The square lattice period is approximately 355 nm. The height of the perforated membrane is about 340 nm.

This system supports high-Q symmetry-protected bound states in the continuum (BIC) at the Γ -point with zero radiative losses due to symmetry mismatch and consequently zero overlap between the even mode profile inside this structure and external electromagnetic propagating modes [36, 56, 57].

This resonant mode is visible in the wavelength range from 900 to 1000 nm in the experimental reflection spectra, which is in good agreement with the analytical calculations obtained by our colleagues using the COMSOL Multiphysics package, as well as the Fourier modal method (Figure 1 b)).

As can be seen from the reflection map, as the angle of incidence increases, the radiative losses in such a system rise and, consequently, the resonant mode broadens, while in the vicinity to normal incidence, where the symmetry-protected mode exists, the radiative losses of the system are close to zero, and the spectral dip vanishes.

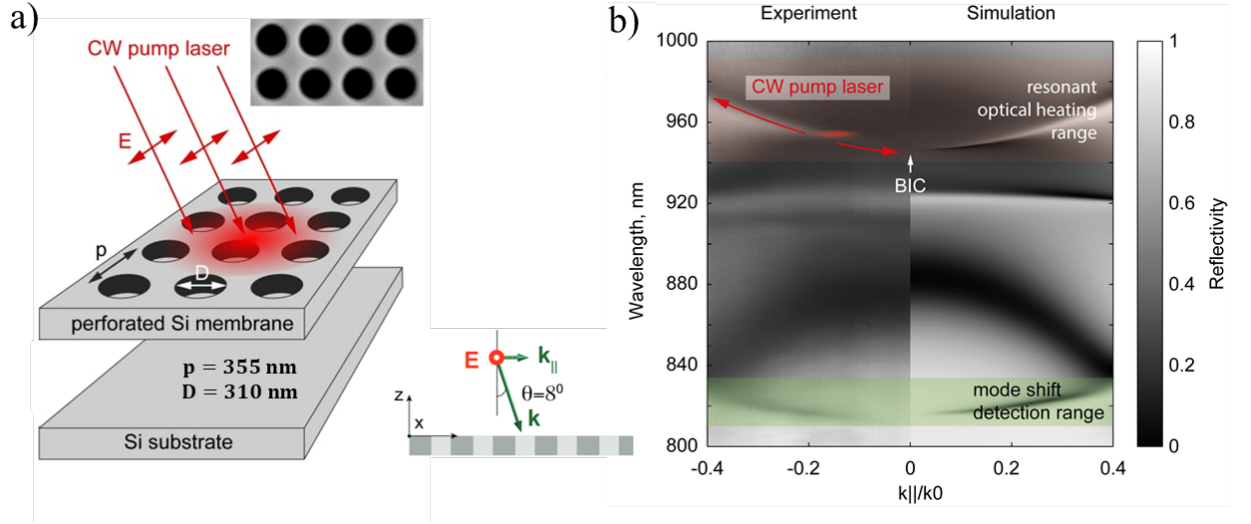


Figure 1 — a) Scheme of the studied perforated silicon membrane with slightly conical holes illuminated by continuous laser radiation at different angles of incidence. b) Reflection map obtained experimentally (on the left) and numerically (on the right) of the membrane under study for various angles of incidence (wave vector projections) and wavelengths. The upper mode corresponds to the symmetrically protected bound states in the continuum. The lower green region shows the mode, the thermo-optical shift of which was used in Section 4.2 to determine the structure temperature

Excitation of such a resonant Q-BIC mode at different angles of incidence makes it possible, first of all, to realize high efficiency of optical heating inside this structure. Moreover, by changing the angle of the incident pump and the laser wavelength, one can also control the frequency detuning $\Delta\omega$, the total γ and the radiation losses γ_r in such a system, which is necessary to switch the resonant mode to bistability regime.

Besides that, it is important to note that, due to the membrane configuration, this structure provides not only a high quality factor of the excited optical modes, but also eliminates the problem of heat outflow through the substrate. These two factors undoubtedly increase the efficiency of optical heating, which indicates the promise of using membrane structures for various applications.

4.2. Temperature estimation

One of the objectives of our theoretical study was the processing of experimental data from thermometry methods in order to obtain the real temperature evolution of the structure at various laser powers.

The temperature increase caused by the laser was determined by the experimenters in two ways: Raman thermometry and observation of a red spectral shift for another optical mode in the membrane at about 815 nm (Figure 1 b)).

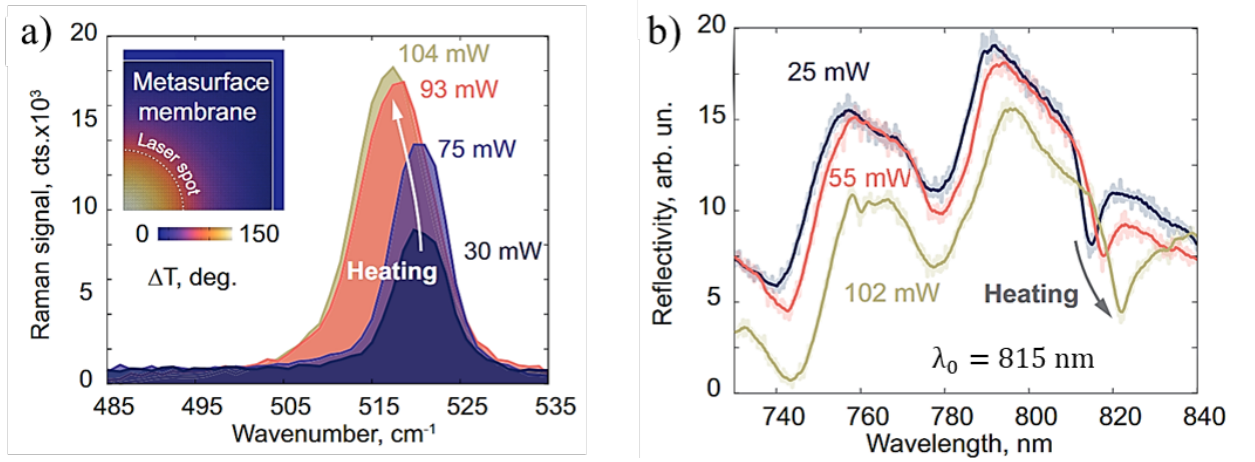


Figure 2 — a) Temperature-induced Raman shift measured under the action of laser radiation of various incident powers at wavelength of 958 nm on described membrane at 4 degrees ($k_{||}/k_0 = 0.07$). The inset corresponds to the estimated temperature distribution in metasurface membrane under laser heating. b) Temperature-induced spectral shift of the optical mode $\lambda_0 = 815$ nm, shown as the reflectivity evolution for metasurface heated by CW laser at different powers at wavelength of 960 nm and 8 degrees ($k_{||}/k_0 = 0.14$) angle of incidence

We convert the data obtained by these approaches using the underlying theoretical basis.

First of all, we extract the temperature from the spectral shift of the Raman peak shown in Figure 2 a), using the following expressions [58]

$$\Omega(T) = \Omega_0 + A \left(1 + \frac{2}{e^x - 1} \right) + B \left(1 + \frac{3}{e^y - 1} + \frac{3}{(e^y - 1)^2} \right),$$

where $\Omega_0 = 528 \text{ cm}^{-1}$, $A = -2.96 \text{ cm}^{-1}$, $B = -0.174 \text{ cm}^{-1}$, $x = \hbar\Omega_0/2kT$, $y = \hbar\Omega_0/3kT$ for crystalline silicon.

On the other hand, we also convert the spectral shift towards higher wavelengths for the 815 nm optical mode (Figure 2 b)), caused by the temperature-dependent increase in the refractive index of silicon, into a heating value.

Indeed, due to the temperature rise inside the metasurface, induced by the laser radiation at wavelength of 960 nm and angle of incidence about 8 degrees ($k_{||}/k_0 = 0.14$), the refractive index of the material for another optical mode about 815 nm also increases, as we mentioned earlier

$$n(\Delta T) = n_0 + n_1\Delta T$$

where $n_0 = 3.6822$ [59], $n_1 = 3.315 \cdot 10^{-4} \text{ K}^{-1}$ [22] for crystalline silicon at 815 nm wavelength.

Therefore, the temperature rise in the system can be found by substituting the values of the resonant wavelength shift and the above material properties of Si from this expression

$$\frac{\Delta\lambda}{\lambda_0} = \frac{\Delta n}{n_0} = \frac{n_1\Delta T}{n_0},$$

$$\Delta T = \frac{\Delta\lambda \cdot n_0}{\lambda_0 \cdot n_1},$$

where $\Delta\lambda$ - redshift of the optical mode during heating.

4.3. Temperature evolution of metasurfaces

We use methods described in Section 4.2 in order to estimate the membrane temperature under laser irradiation. So, the Figure 3 shows the comparison of data obtained from Raman thermometry and from the observation of the mode redshift at a wavelength of 815 nm (green and black curves respectively), which confirms the fairly good agreement between these two described methods. The small difference in the hysteresis boundaries can be caused by slight variations in the excitation conditions.

Since the two approaches give similar temperature dependences, the main experimental results were obtained using spectral shift thermometry, since this method is much more convenient in the utilized experimental geometry.

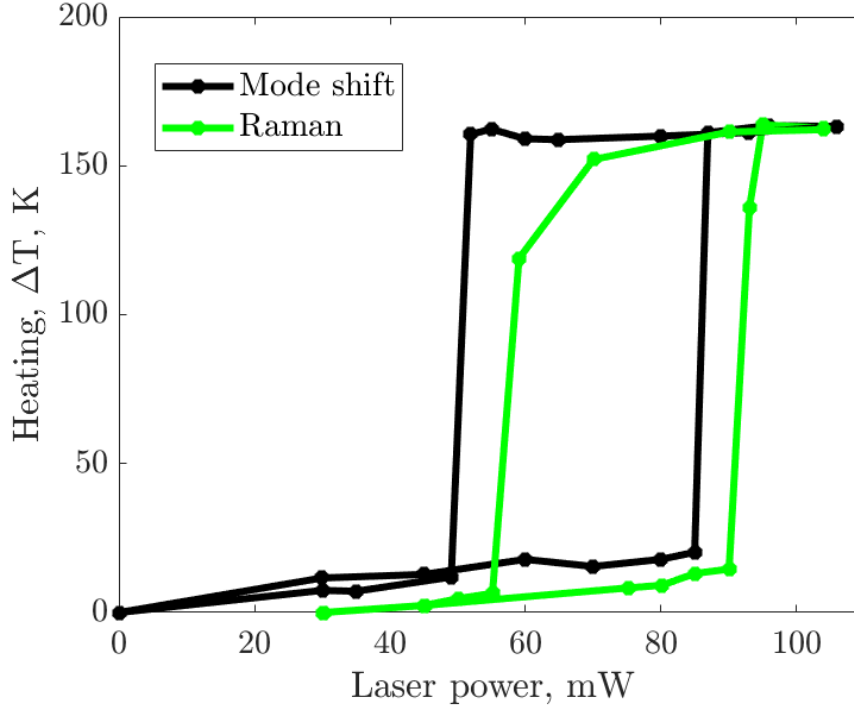


Figure 3 — The temperature hysteresis loop observed in the experiment at $\lambda = 958$ nm and $k_{\parallel}/k_0 = 0.07$ and measured using Raman thermometry (green line) or based on the temperature-induced spectral shift of the reflectance (black line)

So, in the Figure 4 one can see the temperature evolution during laser power cycling in ascending and then descending sequence for various detunings between laser line and BIC mode and different angles of incidence.

The points corresponding to the excitation conditions, in which the temperature evolutions were experimentally measured, are marked on the reflection map, which is shown in the Figure 4 a).

As can be seen from the Figure 4 b), the shape of the curves for this heating evolution during the passage in the forward and reverse directions with respect to the power increase strongly depends on the frequency detuning, as well as on the incidence angle.

Heating curves modifications with incident angle variation is associated mainly with varying radiation losses as the longitudinal projection of the wave vector k_{\parallel} increases. Indeed, as mentioned earlier in a qualitative sense and will be shown in the next section in a quantitative sense, the radiative loss of the optical mode for our membrane depends

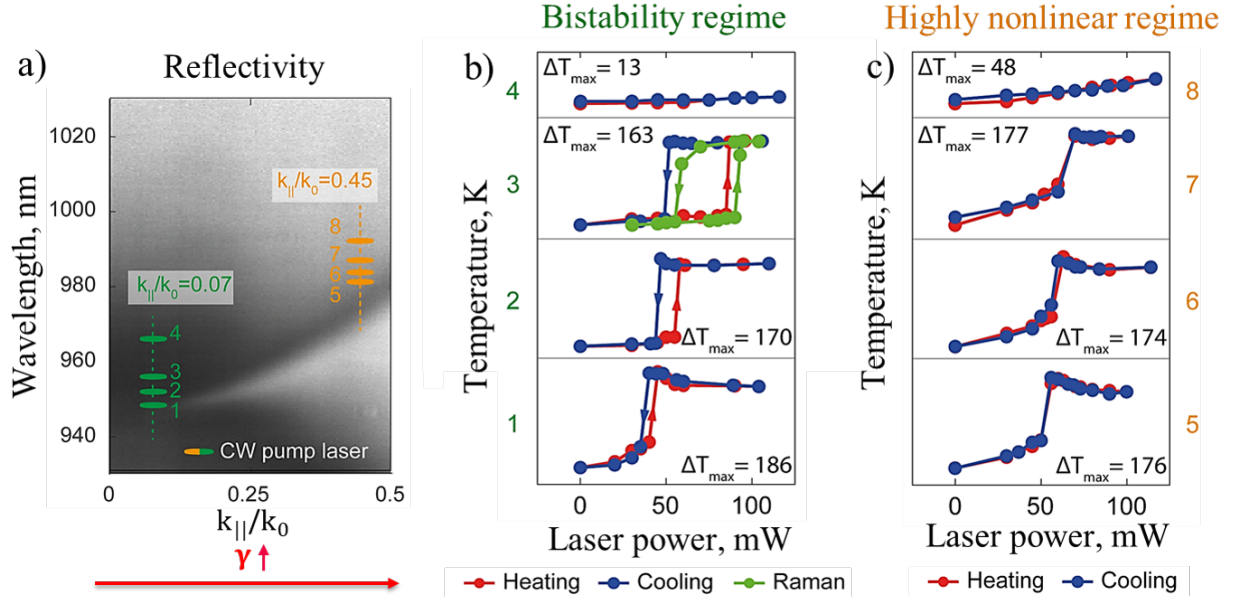


Figure 4 — Reflectivity map depending on incident wavevector projection and frequency. The excitation parameters marked in green correspond to the bistability regime, while the orange ones refer to highly non-linear response of the system. The membrane temperature evolution as a function of the laser power for increasing (red) and decreasing (blue) sequence for bistability regime (b) and strongly nonlinear regime (c). The temperature were extracted by the spectral shift of reflectivity, which is the second method of temperature estimation described in Section. The green curve for point 3 corresponds to the temperature obtained from Raman thermometry measurements

strongly on the $k_{||}$ excitation vector due to the presence of a symmetrically protected BIC at the Γ -point.

Moreover, various curves of temperature dependence on the incident power, illustrated in the Figure 4 b-c) are in good agreement with the theory. Actually, in accordance with the model of a single-mode resonator, in order to observe the hysteresis nature of the temperature evolution, the bistability condition must be satisfied.

Here we consider the bistability condition 5 for the nonlinear thermo-optical coefficient $b = 0$, since for the wavelengths at which we work, the losses shift is negligibly small, that can be obtained by substituting the silicon material parameters into Equation 10.

Therefore, at small angles of incidence $k_{\parallel}/k_0 = 0.07$ due to small losses, thermal bistability exists (Figure 4 b)), since the bistability condition $\Delta\omega/\gamma > \sqrt{3}$ is fulfilled for all frequency detunings.

At the same time, at large angles $k_{\parallel}/k_0 = 0.45$ and the same detunings, the bistability mode is not observed (Figure 4 c)) due to the losses growth with increasing angle of incidence and, consequently, tuning out from the bistability condition. So, for such excitation conditions, we can only see a highly non-linear response of the system and a sharp temperature jump as the hysteresis loop collapses.

In addition, one can note that the reached temperatures, extracted from the experimental data, are in the same range as the optically-excited heating, simulated in COMSOL Multiphysics package with the optical heating module, demonstrated in the inset of the Figure 2 a).

4.4. Fitting metasurface parameters

This section describes the fitting methods by which we find the parameters of the resonant mode of the membrane in order to theoretically estimate the parameters of hysteresis at various settings of frequency detuning and loss.

First of all, we extracted the mode parameters such as total loss and resonant wavelength (or frequency) for considered BIC mode from the reflection map using Fano formula [60]:

$$\sigma = \frac{(\epsilon + q)^2}{\epsilon^2 + 1} \quad (1)$$

where $\epsilon = (\omega - \omega_0)/\gamma$ is the reduced frequency, ω_0 is the resonance mode frequency, γ is the linewidth (total loss) of the mode, q is the phenomenological line shape asymmetry parameter.

The Figure 5 depicts the experimental reflectance data and its fitting basing on the formula for Fano resonance profile.

Fano fitting is used because we are dealing with an asymmetric Fano resonance profile corresponding to the interference of two resonances with different damping coefficients supported by the developed system - the BIC mode and the Fabry-Perot mode between the membrane and the substrate.

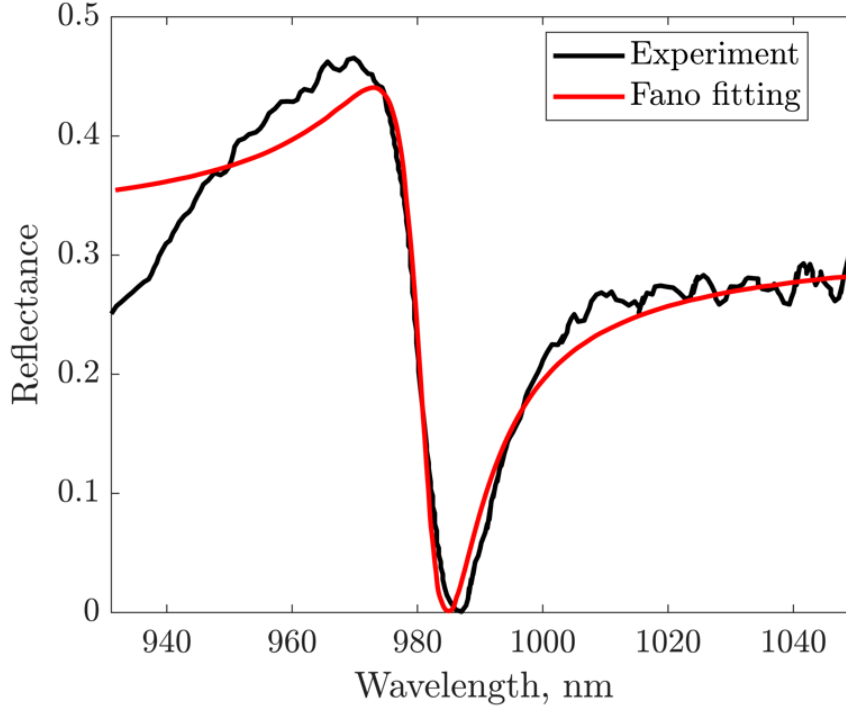


Figure 5 — Experimental (black line) and Fano fitting (red line) data of the reflection coefficient obtained from the membrane excited by external pumping at angle of incidence of about 0.32. The resonant mode parameters extracted by this method are as follows: $\omega_0 \approx 1.96 \cdot 10^{15}$ rad/s, $\gamma \approx 10.87 \cdot 10^{12}$ rad/s

The extracted frequency and loss parameters are indicated in the Figure 6 by black solid lines. It can be noted that, near the Γ -point, the extraction of parameters becomes impossible due to very low radiation losses in the vicinity of the symmetry-protected BIC mode. In addition, the Fano fit does not allow distinguishing of the radiative and non-radiative losses in the system.

Therefore, we also use another method of approximation the mode characteristics and select the mode parameters depending on the angle of incidence so that the theoretical hysteresis width calculated numerically from the Equation 6 coincides with the experimentally obtained one. The values found by this method are displayed as red hollow circles in the Figure 6.

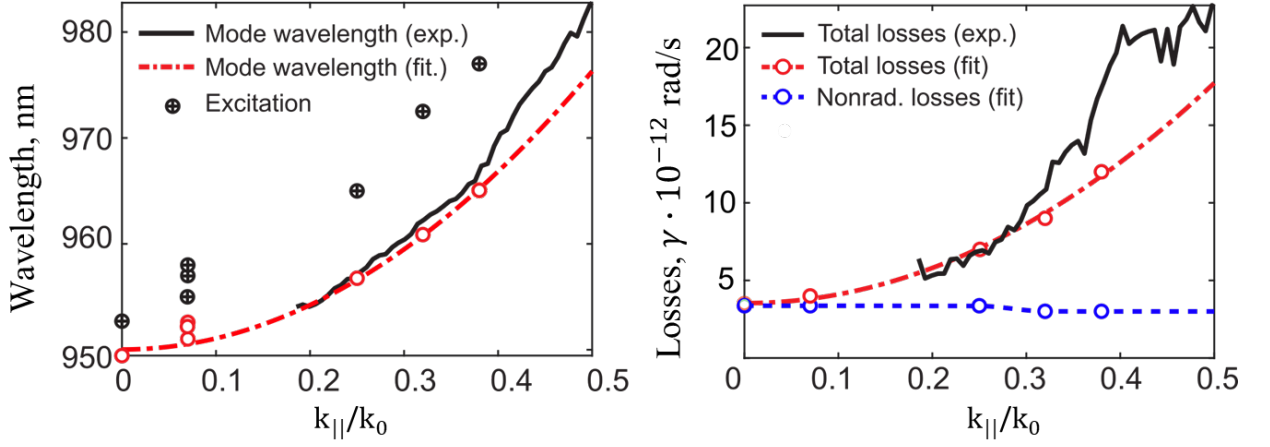


Figure 6 — BIC parameters. a) Resonance wavelength depending on the projection of the wave vector (angle of incidence). The parameters extracted from the experimental reflectivity measurements using Fano formula are indicated by a black solid curve, and the fitted values are shown by red circles connected by a red dotted curve. The excitation wavelength used in experiment is also shown in this graph in crossed cycles. b) Total and nonradiative optical losses as a function of the projection of the wave vector (angle of incidence). The experimental parameters are shown with a black solid curve. The fitted non-radiative loss and their interpolation are in blue, while the total loss are in red

After that, we interpolate the obtained data over the entire range of incidence angles, and near zero we extrapolate frequency curve $\omega_0(k)$ by a quadratic dependence.

It is worth mentioning that not only the total losses and frequencies of the resonant mode are selected by this method, but also the corresponding non-radiative losses, shown by the blue curve. The obtained nonradiative losses of the resonant optical mode are practically independent of the angle of incidence, which is well described by theory.

Finally, as can be seen from these plots, the mode dispersion obtained by two different methods is in good agreement with each other. Therefore, for further analysis, we work with hysteresis-based approach of experimental parameters. With this method we use data on frequencies and total losses, extrapolated at small angles of incidence, as well as calibrated via hysteresis width correspondence non-radiative losses.

Using the above data, one can, first of all, reconstruct the hysteresis loop analytically and make sure that it describes the experimental observation well (Figure 7).

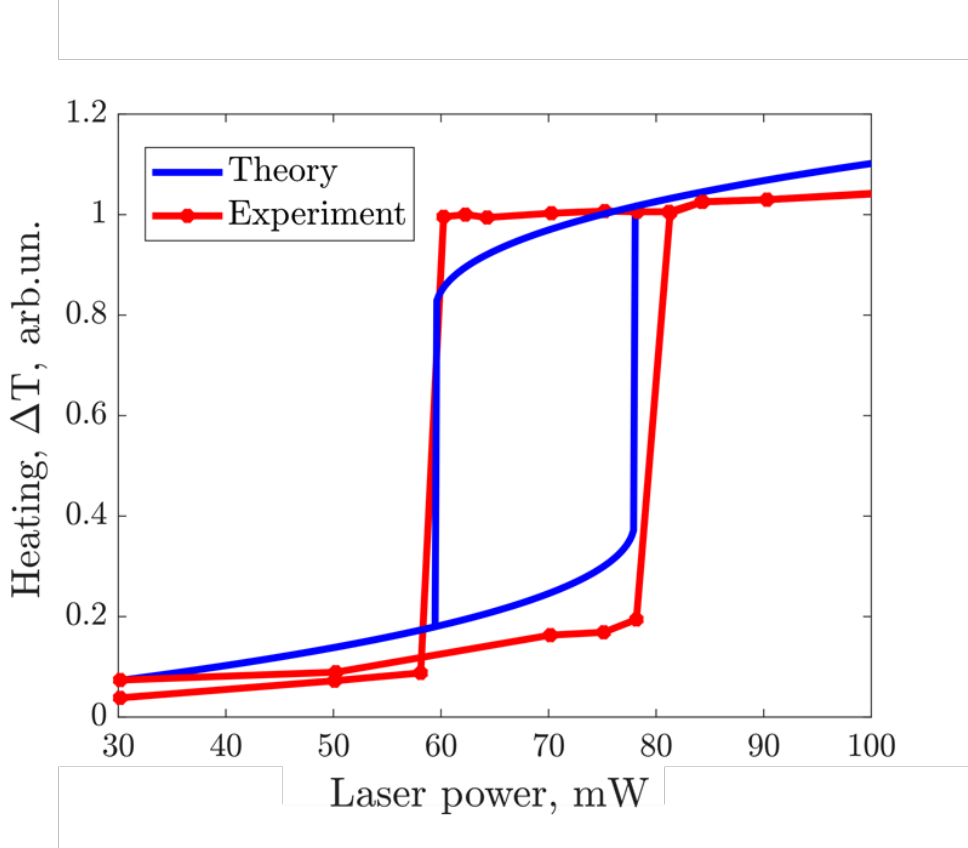


Figure 7 — Dependence of the metasurface temperature on the excitation intensity in the bistability regime for incident excitation at $k_{\parallel}/k_0 = 0.25$ and $\lambda = 965$ nm. The results provided by the theoretical model are shown as a solid blue line, and the experimental hysteresis is marked in red

In addition, based on the described data for resonant wavelength and loss, we also estimate the hysteresis width for various angles of incidence (k_{\parallel}/k_0) and detuning $\Delta\gamma$ using the theoretical Equation 6 for W_h obtained in the 2.3 section. Thus, the calculated map is shown in the Figure 9.

As mentioned earlier, since in the experiment we are dealing with limited pumping, in this case $P_{max} = 100$ mW, the switching power P_{up} to the upper state must not exceed the threshold power P_{max} to maintain the hysteresis.

Therefore, the real width of the hysteresis shown in the Figure 8 is restricted from below by the condition for the occurrence of bistability,

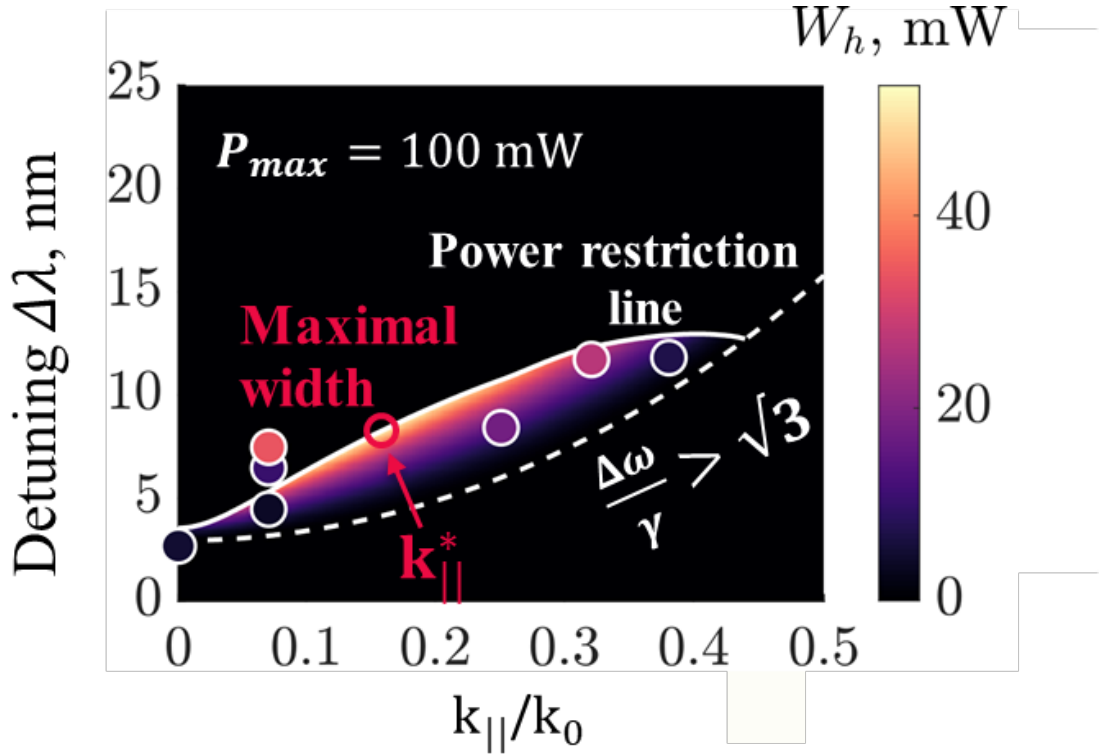


Figure 8 — Estimated map of the width of the hysteresis loop for various detunings and angles of incidence. The white lines indicate the region where bistability is expected to be observed in the experiment, according to the theoretical map 1. The experimentally obtained values are indicated by white circles, the color of which shows the measured hysteresis width. The maximum of the calculated map is shown by the red circle and corresponds to the same projection of the wave vector, which is indicated in Figure 9

and from above by the line corresponding to the threshold power $P_{max} = 100$ mW, similarly to how it was predicted previously in the Section 3.1 from the theoretical point of view.

The experimental values of the hysteresis width are shown in this map with red circles and in the same color bar as the theoretically predicted data underlying this map. Some discrepancy between them can be caused by not accurate extraction of the mode parameters due to the impossibility of fitting the mode lineshape according to the Fano formula in this range of incidence angles, as mentioned earlier. In addition, it can also be connected with the increase in the excitation power for smaller angles of incidence due

to better focusing and lower losses in the objective. This fact may eventually lead to hysteresis loops observed at higher detuning values.

4.5. Critical coupling in metasurfaces

Finally, we verify our derived in Section 3.3 critical coupling condition $2\gamma_r = \gamma_{nr}$ that determines the maximum possible width of the bistability region for fixed threshold power P_{max} for our membrane as follows.

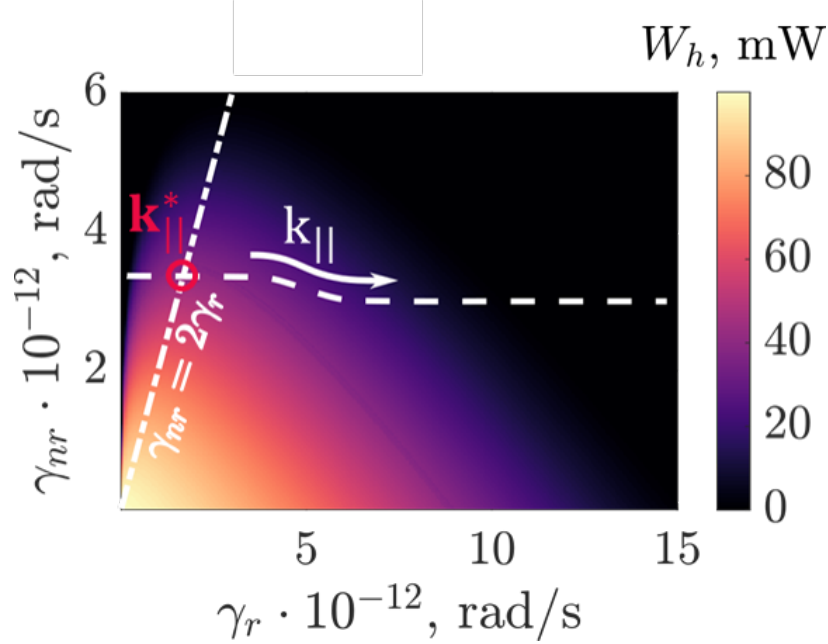


Figure 9 — Map of the hysteresis as a function of radiative and non-radiative losses, demonstrating the non-linear critical coupling condition (white dot-dash line). The white dashed curve corresponds to the ratio between radiative and nonradiative loss in our membrane as the angle of incidence increases. Its intersection with the critical coupling line is highlighted in red and denotes the wave vector projection $k_{||}^*$, relating to the maximum possible hysteresis width that can be obtained in the membrane

The dotted line in the Figure 9, which shows the hysteresis width as a function of losses, marks the dispersion of losses in the structure under study with increasing angle of incidence. Its intersection with the critical coupling line determines the condition for the maximum hysteresis width in our membrane and corresponds to the optimal angle of incidence $k_{||}^*$ highlighted in red.

And it can be seen from the Figure 8 that this angle of incidence, marked with a red circle, really corresponds to the maximum of the calculated hysteresis width map.

Therefore, our theoretical model predicts not only the boundaries of the existence of hysteresis, its width, and also determines the condition for maximizing W under the limitation of the power $P < P_{max}$ that arises in experimental applications.

CONCLUSION

In conclusion, we would like to emphasize that this work, based on the developed theoretical model, identifies the path to achieve the bistability regime in real experimental systems, which can be used in many different applications. So, to obtain the bistability regime in the system, it is necessary:

- to satisfy the bistability condition
- to adjust laser power range to such P_{max} , that $P_{up} \leq P_{max}$

In addition, this study also found a way to achieve the maximum width of the bistability loop and put forward a non-linear critical coupling condition $\gamma_{nr} = 2\gamma_r$.

Moreover, using the developed model, we verify the experimental results measured by our MPTI colleagues and note that since thermo-optical bistability regime is based on a delicate balance between radiative and ohmic losses of the system, BIC metasurfaces offer a unique platform for controlling optical bistability.

The strong dependence of the optical mode linewidth on the projection of the wave vector in the vicinity of BIC allows to control the nature of the nonlinear response and makes it possible to switch the system from a strongly nonlinear response to the hysteresis regime.

In addition, hysteresis loop parameters such as hysteresis width and threshold power can be modified by balance the ratio between radiative and non-radiative loss, which is a unique attribute of BIC in metasurfaces.

Finally, this approach makes it possible to optimize the width of the hysteresis loop, which corresponds to the obtained mode of the nonlinear critical coupling condition.

Thus, summing up this work, we can state that the main steps and results of this study are the following:

- creation of the theoretical model of a single-mode resonator to describe the thermo-optical heating of a nanostructure in linear and non-linear (taking into account the thermorefractive effect) cases;

- derivation of the critical coupling condition for the connection between radiative and nonradiative losses, which maximizes heating in the linear and non-linear cases;
- explanation of thermo-optical non-linearity and bistability in terms of the single-mode resonator model;
- derivation of the hysteresis parameters and the critical coupling condition for the connection between radiative and nonradiative losses, which maximize the hysteresis width and underlie the effective achievement of the bistability regime;
- application of non-linear resonator model to describe temperature evolution inside the dielectric membrane;
- processing of experimental temperature data obtained by two methods of thermometry;
- extraction of resonant mode parameters from the reflection map based on the Fano formula and analytical fitting of resonant frequencies and losses to match the theoretical and experimental hysteresis widths;
- construction of map for hysteresis width in wide range of different angles of incidence and wavelength detuning from the Q-BIC mode for experimentally studied metasurface;
- definition of the maximum value of the hysteresis width that can be achieved in our membrane system and the corresponding optimal angle of incidence.

REFERENCES

1. All-optical control of light on a silicon chip / Vilson R. Almeida, Carlos A. Barrios, Roberto R. Panepucci, Michal Lipson // *Nature*. — 2004. — . — Vol. 431, no. 7012. — P. 1081–1084.
2. Gibbs Hyatt. *Optical Bistability: Controlling Light With Light*. — Cambridge, MA, USA : Academic Press, 1985. — . — ISBN: 978-0-32314864-1.
3. Bistable optical element and its applications / A. Szöke, V. Daneu, J. Goldhar, N. A. Kurnit // *Appl. Phys. Lett.* — 1969. — . — Vol. 15, no. 11. — P. 376–379.
4. McCall S. L. Instabilities in continuous-wave light propagation in absorbing media // *Phys. Rev. A*. — 1974. — . — Vol. 9, no. 4. — P. 1515–1523.
5. Spiller Eberhard. Saturable Optical Resonator // *J. Appl. Phys.* — 1972. — . — Vol. 43, no. 4. — P. 1673–1681.
6. Gibbs H. M., McCall S. L., Venkatesan T. N. C. Differential Gain and Bistability Using a Sodium-Filled Fabry-Perot Interferometer // *Phys. Rev. Lett.* — 1976. — . — Vol. 36, no. 19. — P. 1135–1138.
7. Felber F. S., Marburger J. H. Theory of nonresonant multistable optical devices // *Appl. Phys. Lett.* — 1976. — . — Vol. 28, no. 12. — P. 731–733.
8. Optical bistability in semiconductors / H. M. Gibbs, S. L. McCall, T. N. C. Venkatesan et al. // *Appl. Phys. Lett.* — 1979. — . — Vol. 35, no. 6. — P. 451–453.
9. Lugiato Luigi A. Optical bistability // *Contemp. Phys.* — 1983. — . — Vol. 24, no. 4. — P. 333–371.
10. Thermo-optical bistability with Si nanocrystals in a whispering gallery mode resonator / F. Ramiro-Manzano, N. Prtljaga, L. Pavesi et al. // *Opt. Lett.* — 2013. — . — Vol. 38, no. 18. — P. 3562–3565.
11. Xu Qianfan, Lipson Michal. Carrier-induced optical bistability in silicon ring resonators // *Opt. Lett.* — 2006. — . — Vol. 31, no. 3. — P. 341–343.

12. Optical switching by capillary condensation / Pierre Barthelemy, Mher Ghulinyan, Zeno Gaburro et al. // *Nat. Photonics*. — 2007. — . — Vol. 1, no. 3. — P. 172–175.
13. Regenerative oscillation and four-wave mixing in graphene optoelectronics / T. Gu, N. Petrone, J. F. McMillan et al. // *Nature Photonics*. — 2012. — . — Vol. 6, no. 8. — P. 554–559.
14. All-optical memory based on injection-locking bistability in photonic crystal lasers / Chin-Hui Chen, Shinji Matsuo, Kengo Nozaki et al. // *Optics Express*. — . — no. 4. — P. 3387.
15. Ultrasensitive On-Chip Photonic Crystal Nanobeam Sensor using Optical Bistability / Qimin Quan, Frank Vollmer, Ian B. Burgess et al. // *Optica Publishing Group*. — 2011. — . — P. QThH6.
16. Jiang Xuefeng, Yang Lan. Optothermal dynamics in whispering-gallery microresonators // *Light: Science and Applications*. — 2020. — Vol. 9, no. 1. — arXiv: 1911.06789 Publisher: Springer US.
17. Optimal bistable switching in nonlinear photonic crystals / Marin Soljačić, Mihai Ibanescu, Steven G. Johnson et al. // *Phys. Rev. E*. — 2002. — . — Vol. 66, no. 5. — P. 055601.
18. Barclay Paul E., Srinivasan Kartik, Painter Oskar. Nonlinear response of silicon photonic crystal microresonators excited via an integrated waveguide and fiber taper // *Opt. Express*. — 2005. — . — Vol. 13, no. 3. — P. 801–820.
19. Sun Peng, Reano Ronald M. Low-power optical bistability in a free-standing silicon ring resonator // *Opt. Lett.* — 2010. — . — Vol. 35, no. 8. — P. 1124–1126.
20. Almeida Vilson R., Lipson Michal. Optical bistability on a silicon chip // *Opt. Lett.* — 2004. — . — Vol. 29, no. 20. — P. 2387–2389.
21. Optical bistability and pulsating behaviour in Silicon-On-Insulator ring resonator structures. / G. Priem, P. Dumon, W. Bogaerts et al. // *Opt. Express*. — 2005. — . — Vol. 13, no. 23. — P. 9623–9628.
22. Jellison G. E., Burke H. H. The temperature dependence of the refractive index of silicon at elevated temperatures at several laser wavelengths // *J. Appl. Phys.* — 1986. — . — Vol. 60, no. 2. — P. 841–843.

23. Maier Stefan Alexander. Plasmonics: Fundamentals and Applications. — Springer-Verlag US : Springer US, 2007. — ISBN: 978-0-387-33150-8.
24. Baffou Guillaume, Quidant Romain. Thermo-plasmonics: using metallic nanostructures as nano-sources of heat // Laser Photonics Rev. — 2013. — Mar. — Vol. 7, no. 2. — P. 171–187.
25. Govorov Alexander O., Richardson Hugh H. Generating heat with metal nanoparticles // Nano Today. — 2007. — Feb. — Vol. 2, no. 1. — P. 30–38.
26. Baffou Guillaume, Cichos Frank, Quidant Romain. Applications and challenges of thermoplasmonics // Nat. Mater. — 2020. — Sep. — Vol. 19, no. 9. — P. 946–958.
27. All-dielectric thermonanophotonics / George P. Zograf, George P. Zograf, Mihail I. Petrov et al. // Adv. Opt. Photonics. — 2021. — . — Vol. 13, no. 3. — P. 643–702.
28. Resonant Nonplasmonic Nanoparticles for Efficient Temperature-Feedback Optical Heating / George P. Zograf, Mihail I. Petrov, Dmitry A. Zuev et al. // Nano Lett. — 2017. — . — Vol. 17, no. 5. — P. 2945–2952.
29. Optically resonant dielectric nanostructures / Arseniy I. Kuznetsov, Andrey E. Miroshnichenko, Mark L. Brongersma et al. // Science. — 2016. — Nov. — Vol. 354, no. 6314. — P. aag2472.
30. Bohren Craig F., Huffman Donald R. Absorption and Scattering of Light by Small Particles. — 1998. — Apr. — ISBN: 978-0-47129340-8.
31. Strong magnetic response of submicron silicon particles in the infrared / A. García-Etxarri, R. Gómez-Medina, L. S. Froufe-Pérez et al. // Opt. Express. — 2011. — Mar. — Vol. 19, no. 6. — P. 4815–4826. — 21445117.
32. Mie resonance-based dielectric metamaterials / Qian Zhao, Ji Zhou, Fuli Zhang, Didier Lippens // Mater. Today. — 2009. — Dec. — Vol. 12, no. 12. — P. 60–69.
33. Huygens optical elements and Yagi—Uda nanoantennas based on dielectric nanoparticles / A. E. Krasnok, A. E. Miroshnichenko,

- P. A. Belov, Yu. S. Kivshar // JETP Lett. — 2011. — . — Vol. 94, no. 8. — P. 593–598.
34. Demonstration of Magnetic Dipole Resonances of Dielectric Nanospheres in the Visible Region / Andrey B. Evlyukhin, Sergey M. Novikov, Urs Zywietz et al. // Nano Lett. — 2012. — . — Vol. 12, no. 7. — P. 3749–3755.
35. Subwavelength dielectric resonators for nonlinear nanophotonics / Kirill Koshelev, Sergey Kruk, Elizaveta Melik-Gaykazyan et al. // Science. — 2020. — . — Vol. 367, no. 6475. — P. 288–292.
36. Giant Nonlinear Response at the Nanoscale Driven by Bound States in the Continuum / Luca Carletti, Kirill Koshelev, Costantino De Angelis, Yuri Kivshar // Phys. Rev. Lett. — 2018. — . — Vol. 121, no. 3. — P. 033903.
37. Ultimate conversion efficiency of second harmonic generation in all-dielectric resonators of quasi-BICs in consideration of nonlinear refraction of dielectrics / Tingyin Ning, Tingyin Ning, Xin Li et al. // Opt. Express. — 2021. — . — Vol. 29, no. 11. — P. 17286–17294.
38. Bulgakov Evgeny N., Sadreev Almas F. High- Q resonant modes in a finite array of dielectric particles // Phys. Rev. A. — 2019. — . — Vol. 99, no. 3.
39. High-Q Localized States in Finite Arrays of Subwavelength Resonators / Danil F. Kornovan, Roman S. Savelev, Yuri Kivshar, Mikhail I. Petrov // ACS Photonics. — 2021. — . — Vol. 8, no. 12. — P. 3627–3632.
40. Koshelev Kirill, Bogdanov Andrey, Kivshar Yuri. Meta-optics and bound states in the continuum // Science Bulletin. — 2019. — . — Vol. 64, no. 12. — P. 836–842.
41. Tsoulos Ted V., Tagliabue Giulia. Self-induced thermo-optical effects in silicon and germanium dielectric nanoresonators // Nanophotonics. — 2020. — . — Vol. 9, no. 12. — P. 3849–3861.
42. Cherroret Nicolas, Chakravarty Abhijit, Kar Aravinda. Temperature-dependent refractive index of semiconductors // J. Mater. Sci. — 2008. — . — Vol. 43, no. 6. — P. 1795–1801.

43. Reversible Thermal Tuning of All-Dielectric Metasurfaces / Mohsen Rahmani, Lei Xu, Andrey E. Miroshnichenko et al. // *Adv. Funct. Mater.* — 2017. — Jul. — Vol. 27, no. 31. — P. 1700580.
44. Anapole mediated giant photothermal nonlinearity in nanostructured silicon / Tianyue Zhang, Ying Che, Kai Chen et al. // *Nat. Commun.* — 2020. — Jun. — Vol. 11, no. 3027. — P. 1–9.
45. Nonlinear heating and scattering in a single crystalline silicon nanostructure / Chien-Hsuan Li, Yu-Lung Tang, Junichi Takahara, Shi-Wei Chu // *J. Chem. Phys.* — 2021. — . — Vol. 155, no. 20.
46. Optical tuning of dielectric nanoantennas for thermo-optically reconfigurable nonlinear metasurfaces / Michele Celebrano, Davide Rocco, Davide Rocco et al. // *Opt. Lett.* — 2021. — . — Vol. 46, no. 10. — P. 2453–2456.
47. Gandomkar Mojtaba, Ahmadi Vahid. Thermo-optical switching enhanced with second harmonic generation in microring resonators // *Opt. Lett.* — 2011. — . — Vol. 36, no. 19. — P. 3825–3827.
48. Thermo-optical reshaping of second-harmonic emission from dimer all-dielectric nanoresonators / Olesia Pashina, Kristina Frizyuk, George Zograf, Mihail Petrov // *Opt. Lett.* — 2022. — . — Vol. 47, no. 8. — P. 1992–1995.
49. Opto-thermally controlled beam steering in nonlinear all-dielectric metastructures / Davide Rocco, Davide Rocco, Marco Gandolfi et al. // *Opt. Express.* — 2021. — . — Vol. 29, no. 23. — P. 37128–37139.
50. Enhanced Optical Bistability by Coupling Effects in Magnetic Metamaterials / Jin Yao, Yina Wu, Jie Liu et al. // *J. Lightwave Technol.* — 2019. — . — Vol. 37, no. 23. — P. 5814–5820.
51. Nonlinear optical heating of all-dielectric super-cavity: efficient light-to-heat conversion through giant thermorefractive bistability / Daniil Ryabov, Olesiya Pashina, George Zograf et al. // *Nanophotonics.* — 2022. — . — Vol. 11, no. 17. — P. 3981–3991.
52. Haus Hermann A. *Waves and Fields in Optoelectronics.* — Upper Saddle River, NJ, USA : Prentice-Hall, 1984. — ISBN: 978-0-13946053-1.

53. Frey Bradley J, Leviton Douglas B, Madison Timothy J. Temperature-dependent refractive index of silicon and germanium // Optomechanical technologies for Astronomy / International Society for Optics and Photonics. — Vol. 6273. — 2006. — P. 62732J.
54. Doost Mark Behzad, Langbein Wolfgang, Muljarov Egor A. Resonant-state expansion applied to three-dimensional open optical systems // Physical Review A. — 2014. — Vol. 90, no. 1. — P. 013834.
55. Resonant nonplasmonic nanoparticles for efficient temperature-feedback optical heating / George P Zograf, Mihail I Petrov, Dmitry A Zuev et al. // Nano letters. — 2017. — Vol. 17, no. 5. — P. 2945–2952.
56. Azzam Shaimaa I., Kildishev Alexander V. Photonic Bound States in the Continuum: From Basics to Applications // Adv. Opt. Mater. — 2021. — . — Vol. 9, no. 1. — P. 2001469.
57. Dynamic Nonlinear Image Tuning through Magnetic Dipole Quasi-BIC Ultrathin Resonators / Lei Xu, Khosro Zangeneh Kamali, Lujun Huang et al. // Adv. Sci. — 2019. — . — Vol. 6, no. 15.
58. Balkanski M., Wallis R. F., Haro E. Anharmonic effects in light scattering due to optical phonons in silicon // Physical Review B. — 1983. — Vol. 28, no. 4. — P. 1928–1934.
59. Green Martin A. Self-consistent optical parameters of intrinsic silicon at 300 K including temperature coefficients // Solar Energy Materials and Solar Cells. — 2008. — Vol. 92, no. 11. — P. 1305–1310.
60. Miroshnichenko Andrey E., Flach Sergej, Kivshar Yuri S. Fano resonances in nanoscale structures // Rev. Mod. Phys. — 2010. — . — Vol. 82, no. 3. — P. 2257–2298.

Acknowledgements

The author is grateful to Mihail Petrov, Daniil Ryabov, Olga Sergaeva, Zarina Sadrieva, Ivan Sinev, Alexey Shcherbakov, Andrey Bogdanov for useful and meaningful discussions, as well as Alexander Barulin, Alexander Chernov for conducting the experiment.